MATERIALS CHEMISTRY
FRONTIERS

CCS 中国化学会 CHINESE CHEMICAL SOCIETY
ICCAS
ROYAL SOCIETY OF CHEMISTRY

REVIEW

View Article Online
View Journal | View Issue

Cite this: *Mater. Chem. Front.*, 2023, **7**, 1268

A review of all-solid-state electrolytes for lithium batteries: high-voltage cathode materials, solid-state electrolytes and electrode–electrolyte interfaces

Mingming Ma,[a] Menghui Zhang,[a] Bitao Jiang,[a] Yang Du,[a] Bingcheng Hu *[a] and Chengguo Sun*[ab]

Solid-state electrolytes (SEs) have attracted great attention due to their advantages in safety, electrochemical stability and battery packaging; especially, they can match with high-voltage cathode materials and the Li metal anode to further increase the energy density and electrochemical cycling property. In the past decade, great breakthroughs have been made in the research of electrodes, electrolyte materials and electrode/electrolyte interfaces of high-voltage all-solid-state lithium batteries (ASSLBs). Herein, we summarize the emerging high-voltage cathode materials and their matched solid-state electrolytes; we also analyze the interface problem from a new perspective (corrosion). The authors provide their perspectives on the state of current ASSLBs research, and aim to propose possible research directions for the development of high-voltage ASSLBs in the future.

Received 18th October 2022,
Accepted 11th January 2023

DOI: 10.1039/d2qm01071b

rsc.li/frontiers-materials

1. Introduction

Since the world has entered the new century, the development of renewable energy such as solar energy,[1–3] wind energy[4–6] and ocean energy[7–9] has achieved tremendous progress, and rechargeable batteries as an energy storage device have thus entered a prosperous period. Among them, lithium metal batteries have broad prospects due to their light weight, long service life and low maintenance costs.[10] All-solid-state lithium

[a] *School of Chemistry and Chemical Engineering, Nanjing University of Science and Technology, Nanjing, Jiangsu 210094, China. E-mail: hubc@njust.edu.cn, cgsun@njust.edu.cn*
[b] *School of Chemical Engineering University of Science and Technology Liaoning, Anshan 114051, P. R. China*

Mingming Ma

Mingming Ma is currently a Ph.D student of Nanjing University of Science and Technology. He received a bachelor's degree from Lyuliang University (2017) and a master's degree from Guilin University of Technology (2020). His research focuses on the preparation and research of high-voltage polymer electrolyte materials.

Bingcheng Hu

Bingcheng Hu is a professor at Nanjing University of Science and Techology (NJUST), China, and received his PhD degree in chemical engineering and technology at NJUST in 2005. He had ever worked as visiting scholar in University of Bremen, Germany. His research interests are high-energy energetic materials, photochromic materials and all-solid-state lithium-ion batteries, aiming at preparation of the high-energy-density and high-nitrogen-containing materials, highly reliable photosensitive materials and the high ionic conductivity of solid-state electrolytes.

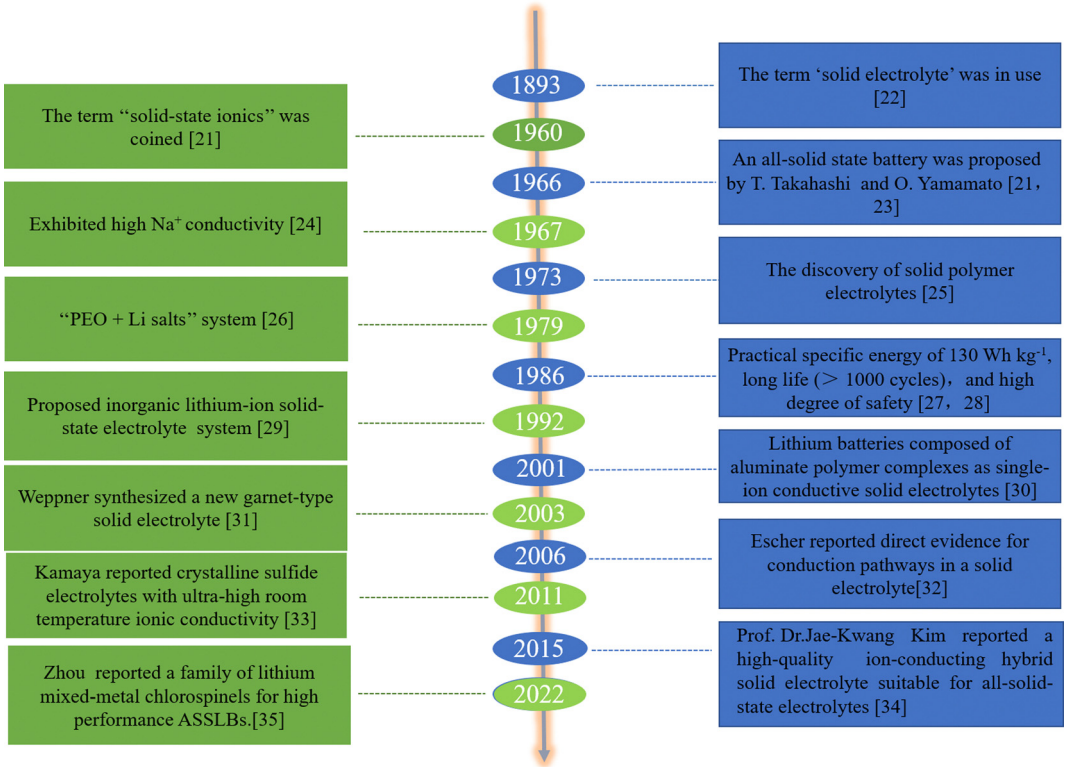

Fig. 1 Early history from solid-state ionic conductors to composite solid-state electrolytes.[21–35]

batteries (ASSLBs) have become one of the important development directions of next generation lithium metal batteries because of their unique advantages of high safety and high energy density.[11] They would develop into the technology that is the focus of attention and competition for scientists and power battery enterprises all over the world.

Compared with traditional liquid lithium metal batteries, the internal structure of solid-state lithium metal batteries is greatly simplified. In the whole battery, the solid electrolyte replaces the liquid electrolyte, the separator and the binder, not only conducting Li^+ during the charging and discharging process, but also acting as a separator to prevent the positive and negative electrodes from directly coming into contact.[12] Meanwhile, solid-state batteries have more advantages and greater development space.[13] First of all, the electrolyte exists in a solid form, and multiple electrodes can be connected in series to prepare a high-voltage single battery. It can also be manufactured in a large-area roll-to-roll manner to improve production efficiency. Secondly, there is no electrolyte leakage or corrosion problems, making the battery safe and environmentally friendly. The solid electrolyte itself is light in weight and high in energy density, which can effectively reduce the weight of batteries and is crucial for practical applications. Thirdly, the solid-state electrolyte has a wide electrochemical window and can be matched with high-voltage cathode materials. Therefore, the selection range of battery materials is significantly broadened, and the power density can also be effectively improved. Finally, solid electrolytes have a long service life and can be used as a soft pack battery. It is precisely because of the unique advantages of solid-state lithium metal batteries that they have considerable potential in many aspects. Fig. 1 summarizes the early history from solid-state ionic conductors to composite solid-state electrolytes.[14] The current research on solid-state lithium metal batteries mainly focuses on the following two aspects. On the one hand, solid-state lithium metal batteries mainly use $LiFePO_4$ as the cathode

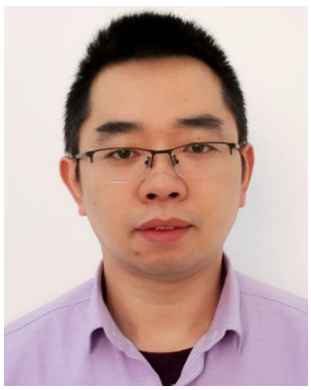

Chengguo Sun

Chengguo Sun is a professor at Nanjing University of Science and Techology (NJUST), China, and received his PhD degree in chemical engineering and technology at NJUST in 2014. He had ever worked as a research fellow in University of Science and Techology Liaoning, and a postdoctoral research fellow at Institute of Metal Research, Chinese Academy of Science. His research interests are high-energy-density materials, electrocatalysts and all-solid-state lithium-ion batteries, aiming at preparation of the energetic cyclo-pentazolate salts and the high ionic conductivity of solid-state electrolytes.

material, which can match the operating voltage range of most solid electrolytes. However, the operating voltage and energy density are still relatively low compared with those of commercial liquid lithium metal batteries. High voltage and large capacity are two important pursuit directions on the positive side, and a high voltage means the transfer of a single electron that can store more energy.[15,16] Large capacity means more charge transfer at the same potential, which can also improve energy density. As the amount of delithiation increases, the difficulty of delithiation also increases, and higher voltages are required to improve energy density and material capacity.[17] On the other hand, the research on solid-state batteries mainly focuses on the interface between the electrolyte membrane and the positive and negative electrodes. Usually, during the first charge and discharge of the battery, the electrode material reacts with the solid electrolyte interface to form an interface film.[18] During subsequent cycling, this film is continuously formed and decomposed, consuming lithium ions in the electrode material that can participate in cycling. It also reacts with the residual solvent molecules in the solid electrolyte components, resulting in attenuation of battery capacity and a decline in cycle performance.[19] Especially in practical applications, lithium metal batteries are inevitably applied under extreme conditions such as high temperature and high pressure. Under such conditions, the physical and chemical processes of the interface between the electrode and the solid electrolyte become more complicated. Therefore, reducing the occurrence of side reactions at the interface between high-voltage electrode materials and solid-state electrolytes is also important for improving the performance of solid-state batteries.[20]

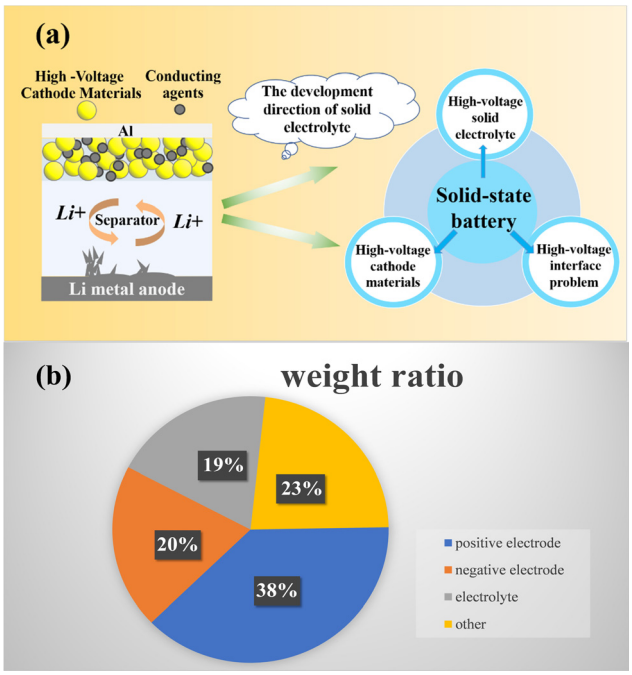

Fig. 2 (a) The development direction of solid electrolytes and (b) a schematic diagram of battery composition with weight ratio.

Considering the importance of solid-state electrolytes for efficient energy storage and conversion in next-generation batteries, it is necessary to summarize the current development of high-voltage solid-state lithium metal batteries (Fig. 2a). In this review, firstly, we introduce the development of high-voltage cathode materials and high-voltage solid-state electrolytes, which are the main components of high-voltage solid-state lithium metal batteries. Secondly, the interface problems between solid electrolytes and high-voltage cathode materials are summarized and analyzed from a corrosion perspective. Finally, the research on high-voltage solid-state lithium metal batteries and interface problems is predicted.

2. Research progress of high-voltage cathode materials

As shown in Fig. 2b, the cathode material accounts for the highest proportion of the battery, about 38% by weight. Therefore, the cathode material has an important influence on the performance of the whole battery. It is one of the most important raw materials in lithium batteries, as it directly determines the safety performance of the battery and whether the battery can be produced on a large scale. At present, the lithium-ion battery uses the cathode material as the lithium precursor, and its cost accounts for more than 30% of the total material cost. Therefore, the preparation of cathode materials with low cost and high energy density is an important goal in the research and production of lithium metal batteries.[36]

At present, high-voltage cathode materials mainly include the spinel structured $LiNi_{0.5}Mn_{1.5}O_4$ (LNMO), layer structured $LiCoO_2$, ternary cathode material Li(Ni, Co, Mn/Al)O_2, lithium rich manganese based cathode material $LiMn_2O_3{\cdot}LiMO_2$ (M = Co/Mn/Ni), olivine structured $LiCoPO_4$ and $LiNiPO_4$ and so on ref. 37. Among them, $LiCoO_2$ and Li (Ni, Co, Mn/Al) O_2 materials have become the focus of attention due to their low cost, high energy density and easy commercialization. Li (Ni, Co, Mn/Al) O_2 materials are the focus of research and development of enterprises and research institutes in various countries, and $LiCoO_2$ is favored by consumer battery product manufacturers. However, there are still some problems with high-voltage cathode materials, including recyclability, power and safety.[38] Table 1 shows some common high-voltage cathode materials. Fig. 3a and b compare the electrochemical performance of some representative high-voltage ASSLBs from the perspectives of capacities under 0.1C and their cycle stability, respectively.

2.1 $LiCoO_2$

$LiCoO_2$ was one of the earliest commercialized layered oxide cathode materials.[47] As one of the main cathode materials for rechargeable lithium metal batteries, $LiCoO_2$ has a high packing density, and its application in 3C electronics dominates.[48–53] As shown in Fig. 4a, $LiCoO_2$ is a layered structure of the α-$NaFeO_2$ type, belonging to the $R\bar{3}m$ space group. The lattice constants are $a = b = 2.816$ Å and $c = 14.052$ Å,

Table 1 Common high-voltage cathode materials

High voltage cathode material	Theoretical capacity (mA h g^{-1})	Actual capacity (mA h g^{-1})	Voltage (V)	Number of cycles	Ref.
$LiMn_2O_4$	148	100–120	3.8–4.25	300	39
$LiCoO_2$	274	200–210	3.0–4.6	100	40
$LiNi_xCo_yMn_zO_2$	285	200–210	2.7–4.3	100	41
$LiNiO_2$	274	140–150	2.5–4.5	100	42
$LiNi_xCo_yAl_zO_2$	279	190–200	3.7	100	43
$LiCoPO_4$	167	90–100	4–5	15	44
$LiNiPO_4$	170	90–100	4.1–5.2	50	45
$LiNi_{0.5}Mn_{1.5}O_4$	148	105–115	3.45–4.95	100	46

Li occupies the 3b site, Co occupies 3a sites, and O occupies 6c sites.[54,55] Among them, the oxygen ions form a cubic close packed structure, and there is a strong interaction between Co and O, which enables layered materials containing Co to have more perfect layered characteristics than those containing Ni or Mn. The theoretical specific capacity of $LiCoO_2$ is 274 mA h g^{-1}. However, the capacity of most $LiCoO_2$ materials is about 140 mA h g^{-1}, which means that only about half of $LiCoO_2$ is deintercalated with Li^+, and the reversible capacity would decrease rapidly when the deintercalation amount of Li^+ exceeds 50%.[56] As shown in Fig. 4b, under 4.2 V, the transition of two hexagonal phases (H1 → H2) occurs at $0.75 < x < 0.95$.[57] At $x = 0.5$, there is a transition from order to disorder in the lithium ions and a transition from hexagonal to monoclinic.[58] In the high-voltage region, $x < 0.2$, the transition of O3 → H1–3 occurs first, followed by the transition of H1–3 → O3.[59,60] As shown in Fig. 4c, during the whole delithiation process, the lattice constant of $LiCoO_2$ increases first and then decreases; especially when the O3 → O1 transition occurs, the *c*-axis shrinks more violently.[61] The lattice oxygen of $LiCoO_2$ participates in charge compensation at high voltage, and a schematic diagram of its energy levels in different delithiation states is shown in Fig. 4d. When the Li content is less than 0.5, the Fermi energy level moves to the region where the Co and O orbitals coincide, and they provide electrons at the same time. Because the oxygen ion is an element constituting the crystal structure, when its valence changes, the whole structure becomes unstable.[62]

In general, a high cut-off voltage can effectively increase the capacity of a material. However, $LiCoO_2$ undergoes an irreversible phase transition during the delithiation process, which leads to problems such as rapid capacity decay and poor long cycle stability.[67] In recent decades, several improved strategies have been reported to improve the cycling stability of $LiCoO_2$ at high voltage. Although some progress has been made, it remains a great challenge to improve the long cycling stability of $LiCoO_2$ at a high voltage of 4.2 V. At present, the mechanism of $LiCoO_2$ capacity fading at high voltage is still unclear.[68] In response to the problems of $LiCoO_2$, researchers have proposed various methods to improve $LiCoO_2$. The long cycle stability, thermal stability and rate capability of $LiCoO_2$ were improved by bulk doping and surface coating of the crystal structure of $LiCoO_2$.[69,70] As shown in Fig. 4e, Zhou[55] studied the attenuation mechanism of $LiCoO_2$ using density functional theory (DFT). In $LiCoO_2$, lithium ions are released during charging, and the volume increases, which can easily cause battery deformation. In particular, the *c*-direction size changes greatly, which leads to an increase of the lithium layer space, so the transition metal ion Co can easily enter the Li layer, resulting in capacity attenuation of $LiCoO_2$. At the same time, an alkaline environment can also lead to degradation of the performance of $LiCoO_2$. As shown in Fig. 4f, Kong[66] reported that the escape of oxygen on the surface of $LiCoO_2$ and the formation of the Li insulator Co_3O_4 are the main reasons for the capacity attenuation of $LiCoO_2$ under high-voltage (4.6 V). The band centers of Co_3d and O_2P were modified by doping MgF_2, while the band gaps of Co_3d and O_2P were enlarged to suppress the escape of surface oxygen and improve the stability of $LiCoO_2$ at 4.6 V.

2.2 High nickel ternary cathode material

After the commercial application of $LiCoO_2$ in 1991, people began to pay attention to and study $LiNiO_2$ and the related high-nickel cathode materials because $LiNiO_2$ and $LiCoO_2$ have similar structures. However, when the temperature is higher than 700 °C, it is difficult to ensure that all Ni is positive trivalent, and some Ni^{2+} is generated, so it is difficult to synthesize $LiNiO_2$ with a strict stoichiometric ratio. In addition, the $LiNiO_2$ structure is seriously mixed with lithium and nickel,

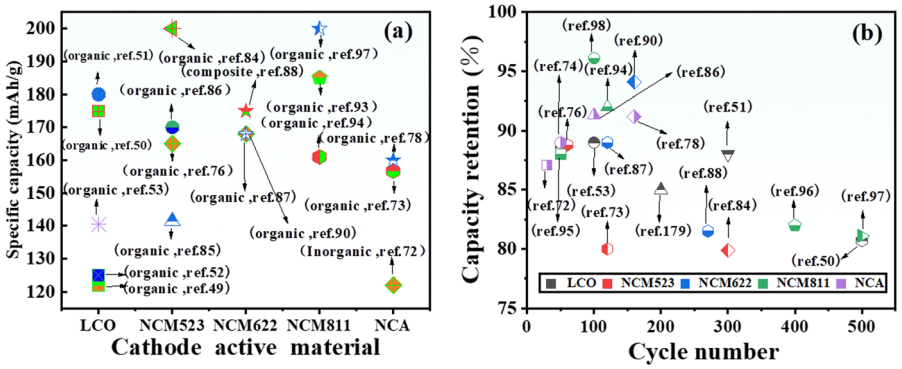

Fig. 3 Electrochemical performance comparison of some representative high-voltage ASSLBs: (a) discharge specific capacities under 0.1C and (b) long-term cycle stabilities.

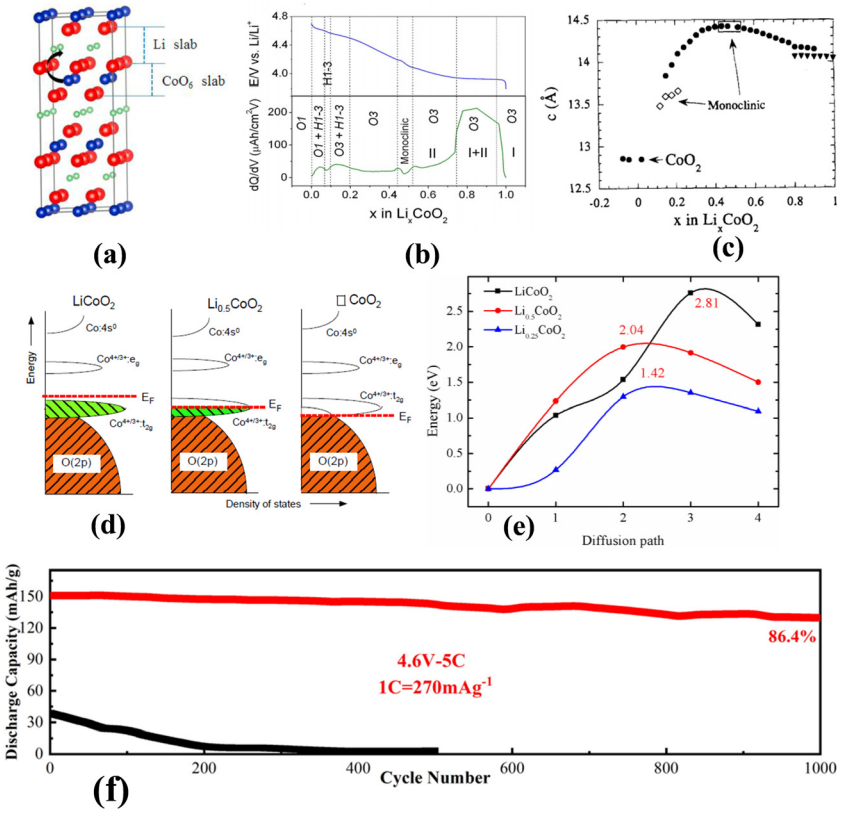

Fig. 4 (a) Schematic diagram of the structure of $LiCoO_2$.[63] (b) Schematic diagram of $LiCoO_2$ delithiation phase transition.[64] (c) Change of the lattice constant *c* during $LiCoO_2$ delithiation.[65] (d) Energy levels of $LiCoO_2$ at different delithiation states.[62] (e) Decay of $LiCoO_2$.[63] (f) Long cycle of MgF_2 modified $LiCO_2$.[66]

resulting in serious capacity fading and poor stability. Modification of $LiNiO_2$ can effectively improve its cycle stability. Deng[71] modified $LiNiO_2$ using trace nano-TiO_2, which can effectively homogenize the size of primary particles, adjust the surface morphology and reduce the specific surface area of materials. This morphological adjustment was conducive to reducing the contact area between $LiNiO_2$ and electrolyte and establishing a stable electrode/electrolyte interface. The trace nano-TiO_2 modified $LiNiO_2$ cathode materials showed good cycle stability. In order to obtain a structurally stable high-nickel cathode material, different elements (Al and Mn)[72–78] have been used to replace part of the nickel, resulting in ternary cathode materials such as $LiNi_xCo_yMn_zO_2$ ($x + y + z = 1$, NCM) and $LiNi_xCo_yAl_zO_2$ ($x + y + z$) = 1, NCAl). Over the past decade, Ni-based transition metal oxides have successfully dominated cathode materials.[79] Compared with an ordinary cathode, a nickel rich cathode has two obvious advantages: a higher specific energy capacity (200–250 mA h g^{-1}) and higher working voltage ($\approx$4.3 V *vs.* Li^+/Li). In 2001, Ohzuku[80] introduced ternary cathode materials into lithium metal batteries for the first time. Since then, ternary cathode materials have begun to develop rapidly. At present, the most commercialized ternary cathode materials in the market are nickel–cobalt–manganese ternary cathode materials. Researchers have used Ni and Mn to partially replace Co in $LiCoO_2$ to obtain the ternary cathode material $LiNi_xMn_yCo_{1-x-y}O_2$ with a layered structure, so as to reduce cost and improve capacity. Its crystal structure is shown in Fig. 5a.[81] In the nickel–cobalt–manganese ternary material, the Ni element plays a major role in the capacity, and both the Co element and Mn element mainly optimize the auxiliary function of the material. It can be roughly divided into two types: the first type is equal. This ternary material has the same proportion of nickel and manganese, and the nickel content is relatively low. There are two kinds of equivalent ternary materials: $LiNi_{1/3}Mn_{1/3}Co_{1/3}O_2$($NCM_{111}$) and $LiNi_{0.4}Mn_{0.4}Co_{0.2}O_2$($NCM_{424}$). In these two types, the valence states of Ni and Co are +2 and +3, respectively, and that of Mn is +4. During charging, divalent nickel ions lose two electrons and are oxidized to tetravalent nickel ions, so the material has higher capacity.[82,83]

The other type is the nickel rich type, which accounts for a high proportion of nickel in cathode materials. There are three types of ternary high nickel cathode materials: $LiNi_{0.5}Mn_{0.3}Co_{0.2}O_2$($NCM_{523}$),[76,77,86–88] $LiNi_{0.6}Mn_{0.2}Co_{0.2}O_2$($NCM_{622}$)[89–94] and $LiNi_{0.8}Mn_{0.8}Co_{0.1}O_2$($NCM_{811}$).[95–100] In these three types of ternary cathode materials, Ni has two valence states, namely +2 and +3, while Co is in its +3 state and Mn still maintains its +4 state, which is used to keep the material structure stable. When the charging voltage is lower than 4.4 V, $Ni^{2+/3+}$ is oxidized to Ni^{4+} in the reaction. However, when the voltage increases, Co^{3+}

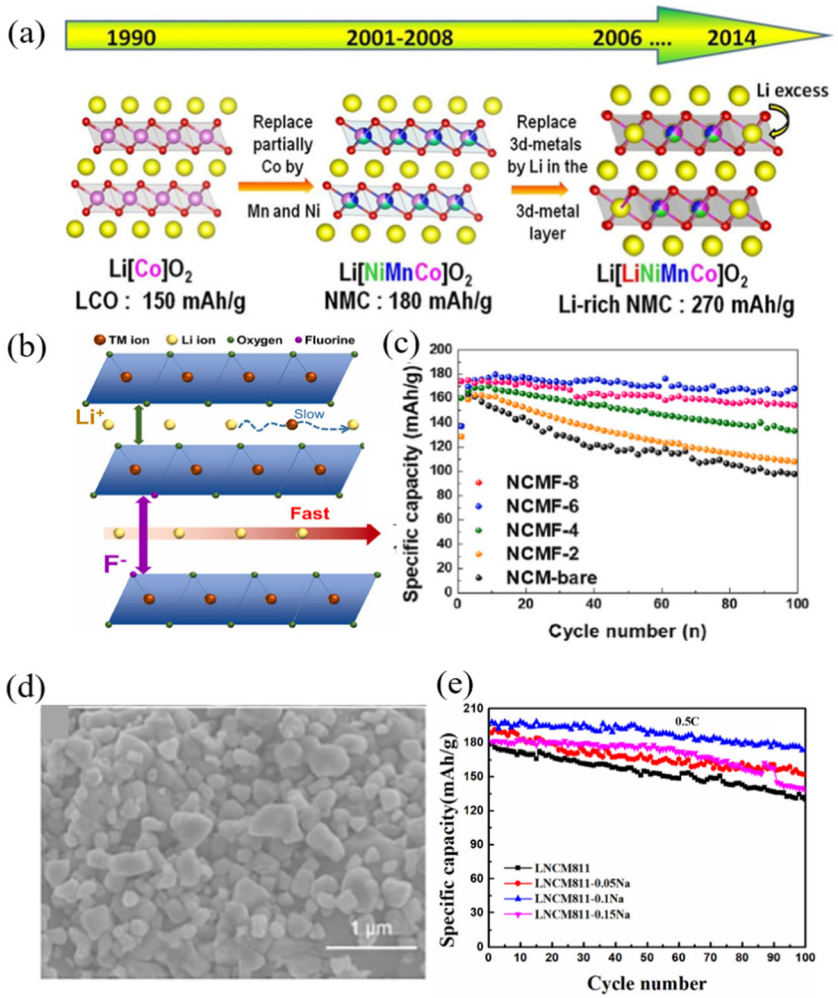

Fig. 5 (a) Schematic diagram of the structure of the ternary cathode material.[81] (b) and (c) Schematic diagram of the structural principle and cycle performance of F-modified NCM.[84] (d) and (e) Microscopy image and cycling performance of Na^+ doped and SiO_2 coated NCM.[85]

participates in the reaction and is oxidized to Co^{4+}.[101,102] With the increase of Ni content, although the storage capacity increases, the electrode stability also decreases, and the high delithiation amount would also destroy the layered structure, resulting in a rapid decline in performance and poor electrochemical stability.[103,104] The higher the Ni content, the easier it is for the surface of the material to react with moisture in the air to generate lithium hydroxide, which in turn reacts with carbon dioxide to generate lithium carbonate. These substances can not only increase the charge transfer resistance, but also generate carbon dioxide by side reactions with the electrolyte during the charging and discharging process, causing potential safety hazards.[105,106] Sung-Beom Kim[84] prepared F-doped nickel-rich ternary cathode materials ($LiNi_{0.8}Co_{0.1}Mn_{0.1}O_{2-x}F_x$) by using different amounts of fluoride as a dopant. Compared with the undoped NCM samples, the F-doped cathode material exhibits improved cycling and rate performance due to the relatively strong bond between the transition metal and F^-, and the improved Li^+ ion transport behavior; however, excess F doping worsened Li^+ migration and reduced the cycling stability of the material (Fig. 5b and c). Zeng[85] improved the cycling stability of the ternary cathode material $LiNi_{0.8}Co_{0.1}Mn_{0.1}O_2$ by a combination of Na^+ doping and SiO_2 coating. Na^+ doping can reduce the shuffling of nickel and lithium, and SiO_2 coating can prevent the active material from being dissolved by the electrolyte during the cycle (Fig. 5d and e). The research results showed that the single-crystal nickel-rich cathode material can achieve a higher energy density and power density in ASSLBs. Yi[107] systematically compared the electrochemical performance of single-crystal $LiNi_{0.6}Mn_{0.1}Co_{0.3}O_2$(SC-$NMC_{613}$) with conventional polycrystalline $LiNi_{0.6}Mn_{0.1}Co_{0.3}O_3$(PC-$NCM_{613}$). The results showed that SC-NCM_{613} had a higher initial specific capacity, better cycling performance and better rate performance in ASSLBs than PC-NCM_{613} even without modification. The poor interface stability between nickel rich ternary cathode materials and the solid electrolyte easily led to poor cycling performance of the ASSLBs. Li[108] coated the $LiNi_{0.8}Co_{0.1}Mn_{0.1}O_2$ cathode material with $LiNbO_3$ to improve the interface stability between the $LiNi_{0.8}Co_{0.1}Mn_{0.1}O_2$ cathode material and $Li_{10}GeP_2S_{12}$ solid

electrolyte. The results showed that the $LiNi_{0.8}Co_{0.1}Mn_{0.1}O_2$ cathode material coated with $LiNbO_3$ exhibited a higher discharge capacity and better cycling performance than the reported oxide electrode material in ASSLBs. Heo[109] encapsulated the $LiNi_{0.8}Co_{0.1}Mn_{0.1}O_2$ cathode material with an amorphous garnet-type solid electrolyte and $La_2(Ni_{0.5}Li_{0.5})O_4$ nanoparticles. Compared with the unmodified $LiNi_{0.8}Co_{0.1}Mn_{0.1}O_2$ cathode material, the performance of the ASSLBs assembled using the oxide-based organic/inorganic hybrid electrolytes was greatly improved.

2.3 Other types of high-voltage cathode materials

2.3.1 High voltage spinel $LiNi_{0.5}Mn_{1.5}O_4$ (LNMO). Spinel lithium nickel manganate ($LiNi_{0.5}Mn_{1.5}O_4$) is one of the high-voltage cathode materials with attractive prospects. Its structure is shown in Fig. 6a. It has a high actual discharge specific capacity, stable structure, high cycle stability, and fast lithium ion conduction and the voltage platform reached 5 V.[110,111] In 2010, Lucht[112] studied the change of cathode–electrolyte interphase (CEI) composition of the LNMO cathode with increasing charging voltage. XPS results showed that the electrolyte (EC/DMC, DEC + $LiPF_6$) is continuously oxidized and decomposed when the first cycle of charging occurs above 4.5 V and the reaction between $LiPF_6$ and the cathode surface is a thermal reaction rather than an electrochemical reaction. The decomposition products LiF and $Li_xPF_yQ_z$ of the lithium salt do not increase significantly. This means the change of CEI is mainly reflected in the increase of EC oxidation decomposition product polycarbonate. During the preparation of LNMO materials, long-time high-temperature calcination was often required, which led to the generation of oxygen vacancies and the appearance of Mn^{3+} ions as compensation for the resulting LNMO cathode materials. Zhu[113] used a wet chemical method to prepare Li_3BO_3 (LBO) coated on the $LiMn_{1.5}Ni_{0.5}O_4$ (LNMO) surface. The LBO coating can prevent the electrolyte from directly etching LNMO, and forms strong chemical interaction with LNMO, which changed the local chemical composition and stabilized the crystal structure of the LNMO active material (Fig. 6b and c). LBO@LNMO maintained a high capacity (76%) even after 1000 cycles at 10C. Wang[114] showed that CuO coating can stabilize the surface structure of LNMO cathode materials.

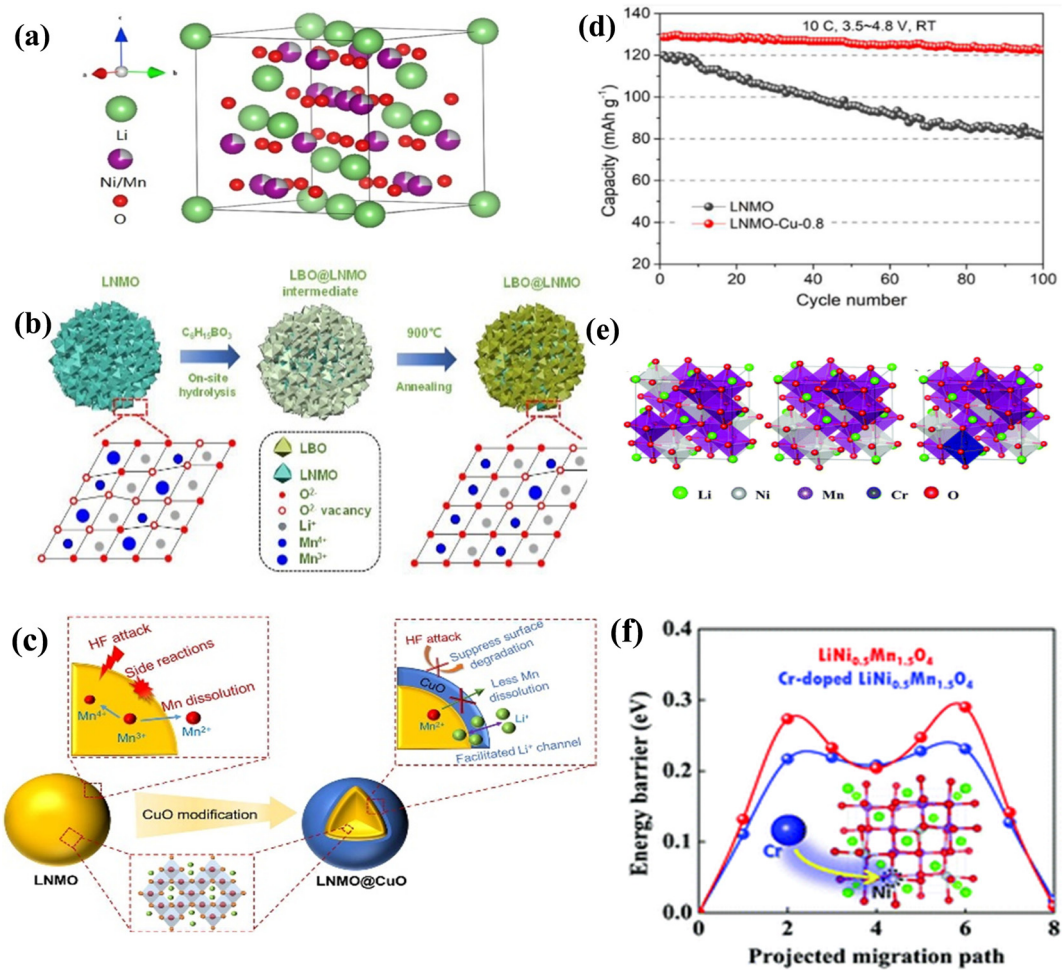

Fig. 6 (a) Schematic diagram of the structure of LNMO.[118] (b) Schematic diagram of LBO modification of LNMO.[112] (c) Schematic diagram of CuO modification of LNMO.[114] (d) The long cycle life of CuO-modified LNMO.[114] (e) Structures of ordered and disordered $LiNi_{0.5}Mn_{1.5}O_4$ with or without Cr doping.[115] (f) Schematic diagram of the structural principle of Cr-modified LNMO.[115]

The CuO coating increased the disordered phase of the LNMO material, accelerated the diffusion of Li^+ and suppressed the dissolution of Mn in LNMO, which enabled excellent cyclic stability (Fig. 6d). Li[115] explored the electrochemical activity, stable configuration and delithiation mechanism at the atomic level by doping Cr in LNMO. The results showed that Cr atoms prefer to replace Ni rather than Mn. The Cr atom preferred to substitute a Ni atom rather than a Mn atom and the configuration with Cr doping has a lower energy in F-$LiNi_{0.5}Mn_{1.5}O_4$ than P-$LiNi_{0.5}Mn_{1.5}O_4$. Cr doping induced a reduction of Mn ions, and the emergence of the reduced Mn ion not only reduced the energy barrier of Li ion diffusion, but also reduced the Li vacancy formation energy (Fig. 6e and f). Shimizu[116] used LNMO cathode materials and a lithium phosphorus oxide nitride (LiPON) solid electrolyte to form a thin-film battery. The battery was still stable after 600 cycles at 5 V-class high voltage, and the average coulomb efficiency was greater than 99%. This showed that LNMO cathode materials can maintain structural stability at 5 V-class high voltage, and have excellent interface stability with a solid lithium phosphorus oxynitride (LiPON) electrolyte. Kim[117] studied the electrochemical properties of LNMO thin films based on the correlation between the ordering of cations (Ni and Mn) in LNMO and oxygen vacancies (V_O). ASSLBs were assembled with the LiPON solid-state electrolyte and thin-film Li anode, and they showed excellent electrochemical performance and good cycle performance.

2.3.2 Lithium-rich manganese-based $LiMn_2O_3{\cdot}LiMO_2$ (M = Co/Mn/Ni) materials. Manganese-based cathode materials are a new type of layered cathode material that can break through the limitation of traditional layered structures and achieve greatly improved specific capacities. Their working voltage is usually 2–4.8 V, which falls in the range of new high-voltage cathode materials. The ordered arrangement of lithium ions and transition metal ions enables additional lithium ions to be introduced into the transition metal layer, thereby greatly increasing the theoretical specific capacity of the material. At present, the specific capacity of lithium-rich manganese-based cathodes is in the range of 280–300 mA h g^{-1}, however the actual reversible capacity of lithium-rich manganese-based materials reported by Xia has reached 400 mA h g^{-1}.[119] The first cycle charge–discharge curve of a lithium-rich manganese-based material is shown in Fig. 7a: the charging curve in the first cycle can be divided into two stages, showing a step-like shape. The slope below 4.4 V is related to the oxidation of Ni and Co, which is similar to ternary cathode materials, and the plateau around 4.5 V corresponds to the oxidation of lattice oxygen. During the first cycle of discharge and subsequent charge and discharge, the oxygen valence platform disappeared, showing an S-type, which is due to the loss of lattice oxygen and structural rearrangement in the first cycle of charge and discharge.[120,121] As shown in Fig. 7b, the Li_2MnO_3 material (monoclinic system, $C/2m$ space group) is the most representative lithium-rich material. In addition to the uniform distribution of lithium ions in the lithium layer, lithium ions are also regularly distributed in the transition metal layer. Manganese-based cathode materials are susceptible to the dissolution of transition metal ions and the escape of oxygen, and their capacity tends to decay rapidly. Zhu[122] constructed a stable layer of $Li_{0.5}Mn_{0.5}O$ (LMO) out of $Li_{1.2}Mn_{0.6}Ni_{0.2}O_2$ (LMNO) using *in situ* acetic passivation and a following calcination process, and the composite material showed prominent rate performance. For lithium-rich manganese-based cathode materials with higher lattice oxygen activity, lattice oxygen is prone to oxidation reactions above 4.5 V, forming the oxidative groups O_2^{n-} (including oxygen), which undergo side reactions with the electrolyte.[123,124] Hong[125] found that Li_2CO_3 decomposed during the first cycle of charge and discharge, and was regenerated during the discharge process. The oxidizing group continuously participated in the reaction to consume the electrolyte, and H_2O was also generated during the whole process, which further formed HF, LiF, POF_3 and other substances; HF can further corrode the surface of the active material. The oxygen absorption reaction mechanism of layered lithium-excess metal oxides in a closed system is shown in Fig. 7c. The results of Yabuuchi[126] were slightly different. They believed that the formation of Li_2CO_3 can improve the cyclability of surface redox reactions, but this cannot be a fully reversible reduction after oxidative decomposition in the charged state. The Li_2CO_3 content was significantly reduced. Nowadays, Li-rich manganese-based materials face problems such as voltage decay, poor rate performance, low compaction density, a wide voltage range and gas production. If all of these problems cannot be effectively solved, the final application of Li-rich manganese-based materials will be limited.

3. Progress on electrolytes for high-voltage ASSLBs

The electrolyte material is an important part of the lithium battery, and the performance of the battery is directly affected by the electrolyte material.[128] Li-metal batteries with liquid electrolytes exhibit good performance, electrical conductivity and interfacial contact.[129] However, liquid batteries have some disadvantages, such as low ion selectivity, insufficient stability and high volatility, especially due to the presence of flammable organic liquids, which have major safety hazards.[130] In recent years, due to the advantages of safety, long cycle stability and thermal stability, all-solid-state batteries have attracted more and more attention, especially because of the obvious safety advantages.[131] Solid electrolytes are mainly divided into three types: inorganic solid electrolytes,[132,133] organic polymer solid electrolytes[134–136] and organic–inorganic composite solid electrolytes.[137,138] In order to obtain a higher energy density than traditional liquid batteries, it is necessary to develop solid electrolytes that can match a higher voltage.[139] This section mainly summarizes the research progress on all-solid-state inorganic electrolytes, all-solid polymer electrolytes and organic–inorganic composite solid-state electrolytes in terms of high voltage capability. Table 2 shows the ionic conductivities and electrochemical stability windows of some representative solid-state electrolytes (SEs) after modification as well as

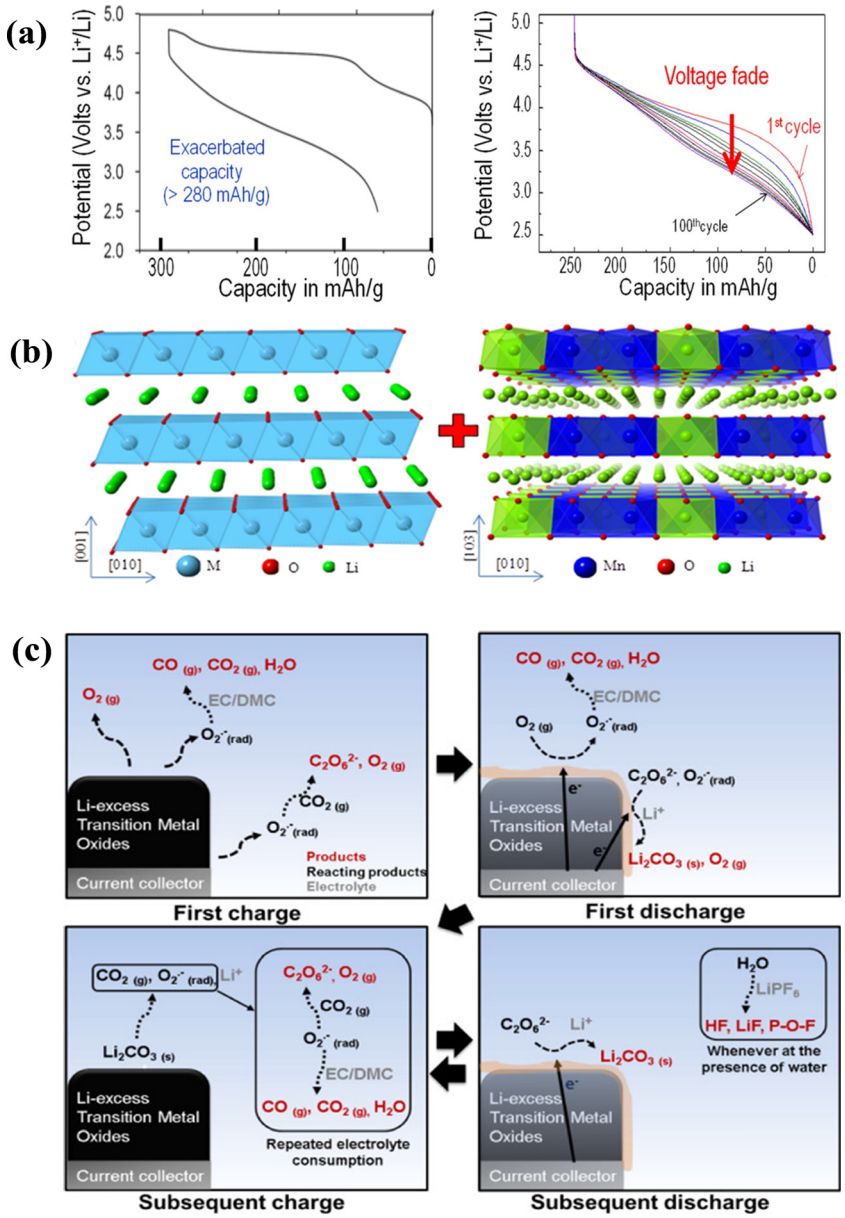

Fig. 7 (a) The first cycle charge–discharge curve of Li-rich manganese-based materials.[127] (b) Schematic diagram of the structure of Li_2MnO_3.[125] (c) Schematic diagram of the reaction mechanism of layered lithium excess metal oxides.[126]

the electrochemical performance of their corresponding high-voltage ASSLBs.

3.1 Inorganic solid electrolytes

A high voltage usually requires a relatively wide operating voltage range (2.5–5.0 V), and a solid electrolyte must have strong anti-oxidation and reduction capabilities within this voltage range, otherwise it cannot remain stable under a high voltage.[159] In recent years, high-voltage inorganic solid-state electrolytes have received more and more attention. Inorganic solid-state electrolytes mainly include oxide solid-state electrolytes, sulfide solid-state electrolytes and other types of solid-state electrolytes. The research results showed that the stable voltage range of an inorganic solid electrolyte obtained experimentally is much wider than the theoretical calculation results.[159] The stable working voltage ranges of the common inorganic solid electrolytes LGPS, LLTO, LLZO, LATP and LAGP calculated by DFT are 1.71–2.15, 1.75–3.71, 0.05–2.91, 2.16–4.31 and 2.7–4.27 V.[160] In experimental studies, the modification of oxide solid electrolytes has mainly focused on the improvement of ionic conductivity and the study of interface problems. It was reported that oxide solid electrolytes can be matched with high-voltage cathode materials without modification.[139,161] Oxide solid electrolytes have been actively explored due to their high Li-ion conductivity and high electrochemical stability.[160,162] The electrochemical window of inorganic oxide solid electrolytes is usually high, such as the electrochemical window of LLZO, which can reach over 5 V.[163,164] However, it is difficult for

Table 2 Ionic conductivities and electrochemical stability windows of SEs after modification and battery performance of resultant high-voltage ASSLBs

Solid electrolyte	Conductivity (S cm^{-1})	Stable window	Cell constitution	Capacity (mA h g^{-1})	Cycle performance	Ref.
PEO + LiTFSI + wheat flour electrolyte	2.62×10^{-5}	—	NCM_{811}/Li	133 mA h g^{-1} (0.1C)	47.3%	140
PMA + PEO	2.05×10^{-4}	—	$LiCO_2$/Li	119 mA h g^{-1} (0.1C)	91.2%	141
PAN + PAN@LAGP + PEGDA	3.7×10^{-4}	0–5 V	NCM_{622}/NCM_{811}/Li	185 mA h g^{-1} (0.5C)	81.5%	142
PEO + SN + LiTFPFB + LITFSI	0.5×10^{-3}	0–5 V	$LiCO_2$/Li	152 mA h g^{-1} (0.1C)	83.5%	143
P(PO/EM) + LITFPFB	1.55×10^{-4}	—	$LiFe_{0.2}Mn_{0.8}$ PO_4/Li	141.1 mA h g^{-1} (0.1C)	92.1%	144
PS/PEG/PS	1.1×10^{-3}	0–4.5 V	NCM_{523}/Li	130 mA h g^{-1} (0.1C)	96.1%	145
Ca–CeO_2/PEO	1.3×10^{-4}	0–4.5 V	$LiCO_2$/Li	113 mA h g^{-1} (0.1C)	70.7%	146
LLZTO/PVDF	2.73×10^{-4}	0–4.77 V	$LiCO_2$/Li	120 mA h g^{-1} (0.1C)	94.1%	147
PAN-*in situ*	3.5×10^{-4}	—	NCM_{622}/Li	177.3 mA h g^{-1} (0.1C)	93.7%	135
PVEC–LITFSI–SiO_2	1.35×10^{-3}	3.0–4.6 V	$LiCO_2$/Li	153 mA h g^{-1} (0.1C)	94%	148
PVA-*g*-PCA-IL-HT	4.78×10^{-3}	0–5.17 V	$LiCO_2$/Li	188.7 mA h g^{-1} (0.2C)	97%	149
PME–LiPVFM–LITFSI	3.57×10^{-4}	0–5 V	$LiCO_2$/Li	196.3 mA h g^{-1} (0.1C)	91.9%	150
PPC–PCDF–LLZTO–LITFSI	1.3×10^{-4}	0–5.1 V	NCM_{811}/Li	200 mA h g^{-1} (1C)	82.8%	151
PTFE + Li_6PS_5Cl + Li_3InCl_6 + LLZTO	5.2×10^{-4}	—	NCM_{811}/Li	173.6 mA h g^{-1} (1/3C)	94.4%	152
$Li_{3-x}Yb_{1-x}Zr_xCl_6$	1.1×10^{-4}	—	NCM_{622}/Li	170.6 mA h g^{-1} (0.2C)	80%	153
PDOL + LiDFOB	2.46×10^{-4}	0–4.9 V	NCM_{811}/Li	175 mA h g^{-1} (0.2C)	—	154
PVAC + TAGDA + AIBN	1.02×10^{-4}	0–5.2 V	NCM_{811}/Li	200 mA h g^{-1} (0.1C)	90%	155
PSiOM	0.41×10^{-4}	0–4.8 V	NCM_{622}/Li	138 mA h g^{-1} (0.1C)	90%	156
PEO + LITFSI + LiI	2.1×10^{-4}	—	NCM_{811}/Li	125 mA h g^{-1} (0.5C)	80%	157
PVEC	2.08×10^{-3}	0–4.8 V	$LiCO_2$/Li	140 mA h g^{-1} (1C)	89%	158

solid-state electrolytes to reach the tested electrochemical window. Han[162] proposed the limited contact area between solid-state electrolytes and noble metals to explain the overestimated electrochemical stability window. The research showed that the interface between LLZO and LNMO started to decompose continuously at 3.8 V. This process promotes phase transition on the surface of the positive electrode and generates $Li_{0.35}Ni_{0.05}NiO_2$, which increases the interface impedance. Eventually, the battery can no longer be charged and discharged.[165] The electrochemical stability window of sulfide solid-state electrolytes is reported to be in the 0–5 V range.[166,167] Research on sulfide solid electrolytes showed that sulfide solid electrolytes and high-voltage cathode materials began to produce decomposition products such as elemental S when the charge is above 3.8 V in the first cycle, resulting in a significant decrease in the coulombic efficiency and a significant increase in polarization in the first cycle.[168] Its decomposition products also increase the interface impedance, and its poor stability prevents the direct use of 4 V-grade $LiMO_2$ (M = Co, Ni, and Mn) cathode materials.[169–171] However, if the sulfide solid electrolyte is not in direct contact with the high-voltage cathode material, it still enables high electrochemical stability. Wang[172] performed sulfide treatment on LNMO (Fig. 8a), and it was reported that the sulfide solid electrolyte could remain stable at a high voltage of 5 V (Fig. 8b). *S* in the sulfide solid electrolyte reacted with water vapor easily to produce an irritating odor and toxic H_2S gas, which led to electrolyte deterioration and failure. Therefore, sulfide solid electrolytes have serious potential safety hazards, and their preparation process needs to be completed in a strict inert atmosphere.

In recent years, some other types of high-voltage inorganic solid electrolytes have also been reported. As shown in Fig. 8c, the $Li_2In_{1/3}Sc_{1/3}Cl_4$ solid electrolyte exhibited excellent electrochemical performance at potentials as high as 4.8 V, and the capacity retention rate was still as high as 80% after 3000 cycles at 3C.[173] The lithium–ytterbium-based halide solid electrolyte (Fig. 8d) can remain stable in the presence of uncoated bare 4 V cathode materials (LCO and NCM_{622}).[174] Zheng[175] generated pure Li_3InCl_6 (LIC) on the surface of $LiCoO_2$ (LCO) by using a vacuum drying assisted method to improve the electrochemical stability of the electrolyte/electrode solid–solid interface and solid electrolyte under high voltage. The assembled ASSLBs showed excellent cycle stability. Kochetkov[176] studied the dynamic evolution of the interface between three different halide solid electrolytes (Li_3InCl_6, $Li_2Sc_{1/3}In_{1/3}Cl_4$ and $Li_{5/2}Y_{1/2}Zr_{1/2}Cl_6$) and the surface of nickel rich NCM_{85} or NCM_{111} cathode material particles, revealing the influence of cation metal substitution on the interface chemistry. The results showed that metals played a key role in determining the high voltage stability. Considering the difference between semi-closed batteries and real batteries, it is important to reveal their electrochemical stability windows in practical solid-state electrolyte applications in the future.[139]

3.2 Organic polymer solid electrolytes

Since soft and porous polyolefin films such as polyethylene (PE) and polypropylene (PP) cannot inhibit lithium dendrite growth, the risk of short circuits cannot be avoided.[177] Polymer solid electrolytes with sufficient mechanical properties, wide electrochemical windows and excellent properties have attracted extensive attention.[177,178] The electrochemical stability of polymer electrolytes varies by type of polymer, lithium salt and test conditions. Table 3 summarizes some common high-voltage organic polymer solid electrolytes. As shown in Fig. 9a and b, a polyvinylidene fluoride (PVDF) electrolyte was modified with tetramethylene sulfone (TMS), and the capacity retention rate of the subsequent battery reached 85% after 200 cycles at room temperature.[179] A solid electrolyte was prepared by mixing bis(oxalic acid) lithium borate(LiBOB) and bis (trifluoromethylsulfonyl) imine lithium salt (LiTFSI) with the solid plasticizer succinonitrile (SN) in poly(ethylene glycol) diacrylate (PEGDA).

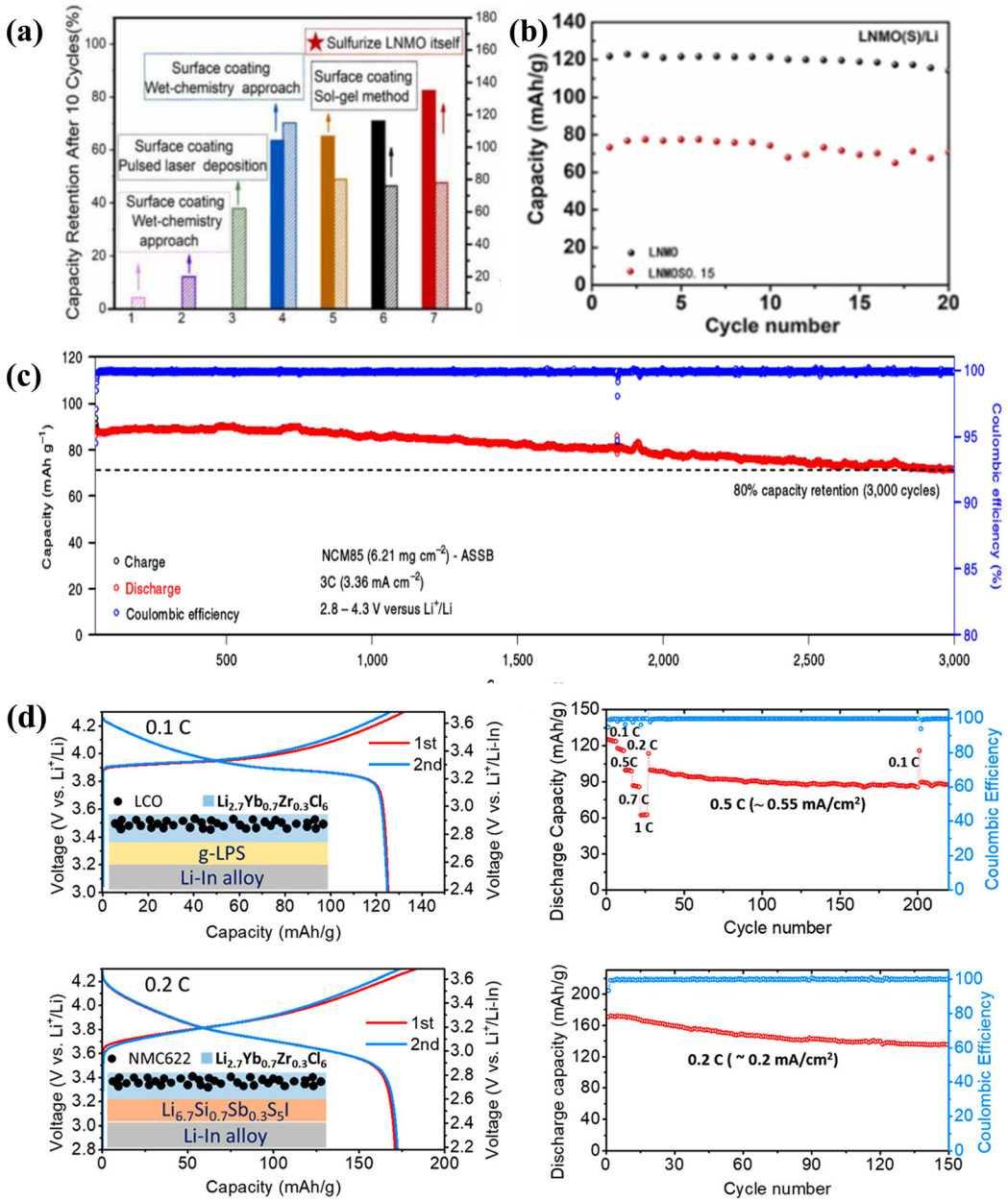

Fig. 8 (a) 5 V-class sulfurized spinel cathode stable in sulfide all-solid-state batteries.[172] (b) $LNMOS_{0.15}$ cycle performance diagram.[172] (c) Long cycle diagram of NCM_{85} ASSLBs (performed after rate cycling) at a rate of 3C.[173] (d) Long cycle diagram of a lithium ytterbium halide solid electrolyte (LCO and NCM_{622}).[174]

Table 3 Common high-voltage organic polymer solid electrolytes

High voltage polymer electrolytes	Molecular formula	Voltage (V)	Number of cycles	Ref.
PPC	—	2.5–4.4	80	181
PVDF	$-(CH_2CF_2)_n-$	3.0–4.5	200	179
PVDF–HFP	$-(CH_2CF_2)_n-(CF_2CF(CF_3)_m-$	3.0–4.3	200	182
PAN	$-(CH_2CH(CN))_n-$	3.0–4.3	200	18

After 1000 cycles at 1C, the average coulomb efficiency exceeded 99.99% and the capacity retention rate was 66% (Fig. 9c and d).[180] Niu[98] prepared a covalent organic framework (COF) based solid electrolyte by introducing lithiophilic groups and electrochemically stable quinolyl aromatic ring linkages. ASSLBs assembled using the COF based solid electrolyte and a nickel rich cathode (NCM_{811}) showed stable cycle performance and a high coulomb efficiency after 400 cycles.

At present, the main methods to improve the electrochemical stability of polymer solid electrolytes are:

(1) Using a polymer with high electrochemical stability as the polymer matrix;

(2) Improving the electrochemical stability of the polymer matrix by cross-linking polymerization and copolymerization;

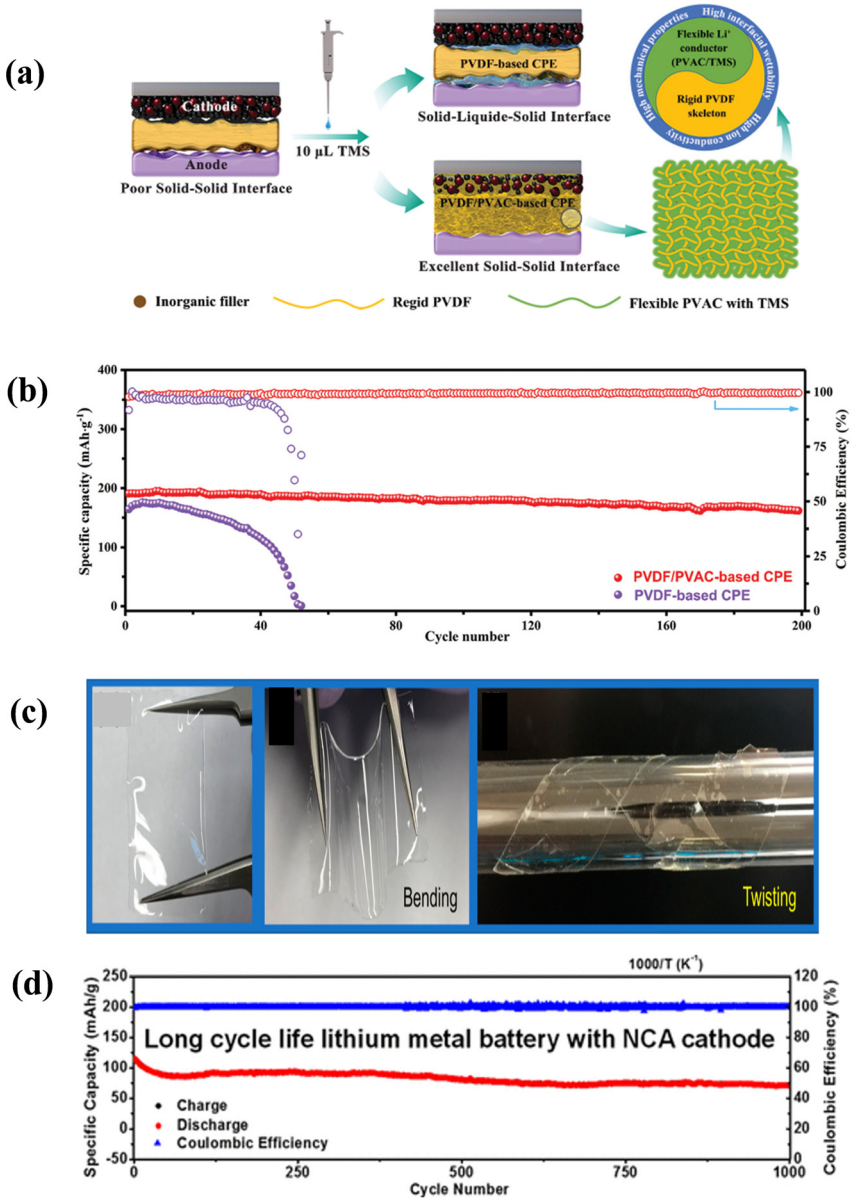

Fig. 9 (a) Schematic diagram of interface modification of a PVDF/PVAC solid electrolyte with TMS.[179] (b) Long cycle performance of a PVDF/PVAC battery.[179] (c) and (d) Photographs of the solid state electrolyte and long cycle performance diagram.[180]

(3) Selecting a suitable lithium salt to improve the overall performance of the polymer, thereby improving the electrochemical stability of the polymer matrix;

(4) Preparing a double-layer or multi-layer electrolyte membrane, with one side of a high-voltage-resistant solid electrolyte close to the high-voltage positive electrode material, and the other side close to the lithium negative electrode;

(5) Synthesis of a new polymer matrix.

3.3 Organic–inorganic composite solid electrolytes

The ionic conductivity of inorganic solid electrolytes is generally good, but their relatively poor mechanical properties and large interfacial impedance between electrodes limit their large-scale applications.[183] Unlike brittle crystalline inorganic electrolytes, polymer electrolytes are lightweight, flexible, scalable and more compatible with advanced manufacturing processes. However, polymer electrolytes also suffer from poor mechanical properties and poor thermal stability.[184] In order to overcome the respective shortcomings of inorganic solid electrolytes and polymer solid electrolytes and take advantage of their respective advantages, recent studies have shown that the performance of batteries assembled with organic–inorganic composite solid electrolytes has been improved to varying degrees.[185–187] With the addition of inorganic materials to the polymer matrix, regardless of whether the filler is active or inactive, the final solid-state electrolytes exhibit stronger electrochemical stability than those without inorganic dopants.[188–190] For example, the electrochemical stability

window of PVDF–LiTFSI is 4.58 V, but when LLZTO is added to the polymer matrix, its electrochemical window increases to 4.82 V.[191] Recent research showed that different fillers had different effects on the electrochemical stability of PEO electrolyte. Zhao[192] added $Li_{6.75}La_3Zr_{1.75}Ta_{0.25}O_{12}$ (LLZTO) to PEO electrolyte. Through the interaction between ceramic particles and polymer matrix, the anion of the electrolyte was effectively fixed, and the electrochemical stability was also greatly improved. The electrolyte showed an electrochemical window up to 5.5 V. Li[193] improved the electrochemical window of PEO electrolyte by adding fluoromethyl modified polyamines to PEO electrolyte. The solid-state battery composed of modified PEO electrolyte and the NCM_{811} cathode material showed excellent cycling performance. The three-dimensional (3D) porous garnet framework reinforced PEO based composite solid electrolyte broadened the electrochemical window of PEO electrolyte, and the ASSLBs assembled with the $LiCoO_2$ cathode material showed excellent cycle stability.[194] However, Lei[195] did not change the electrochemical window of PEO electrolyte after adding SiO_2 to PEO electrolyte. Fan[196] wetted both sides of the inorganic solid electrolyte $Li_{6.35}Ga_{0.15}La_3Zr_{1.8}Nb_{0.2}O_{12}$ (LGLNZO) with PEO electrolyte, and tested the electrochemical window of the composite solid electrolyte. The results showed that the electrochemical window of the composite solid electrolyte was mainly controlled by PEO electrolyte, and LGLZNO particles affected the dynamics of the electrode process.

The main reasons for the enhanced oxidative stability of organic–inorganic composite solid electrolytes are as follows:

(1) Inorganic matter itself has strong oxidation stability;

(2) More anions are adsorbed to the surface of the filler through Lewis acid–base interaction between the polymer and the filler;

(3) Dipole–dipole interactions between fillers and polymers, which can alter the electronic transition energy levels of the latter, increase their oxidative decomposition potential.

Although the electrochemical stability of polymer-based matrices can be improved to some extent by using suitable lithium salts and adding fillers, these enhancements are limited because the inherent properties of polymer matrices do not change drastically. It is more important to use polymers with high electrochemical stability as the matrix to improve the electrochemical stability of polymer electrolytes.

3.4 Emerging composite solid electrolytes for ASSLBs

In recent years, with the development of ASSLBs, some new solid electrolytes have been reported, such as Li/Na-rich antiperovskite (LiRAP/NaRAP) solid-state electrolytes, ultrathin solid-state electrolytes and so on. ASSLBs with Li/Na-rich antiperovskite (LiRAP/NaRAP) solid-state electrolytes exhibited high ionic conductivity and high chemical/electrochemical stability. Deng[197] gave a comprehensive introduction to the development, structural design, ionic conductivity and ion transportation mechanisms, chemical/electrochemical stability, and applications of some antiperovskite materials in energy storage batteries. Zhu[198] used the chemically compatible cellulose membrane as the self-limiting skeleton and designed an ultrathin (60 μm), flexible and free-standing argyrodite (Li_6PS_5Cl) solid electrolyte through the self-limiting strategy. The ASSLBs assembled with different types of cathode (sulfur and lithium titanate) and anode materials (lithium and lithium–indium alloy) showed stable and high-speed performance. Yang[199] provided a comprehensive summary on $Li_{1+x}Al_xTi_{2-x}(PO_4)_3$ (LATP), which was conducive to the development of ASSLBs based on LATP.

4. Research progress on interface problems of high-voltage ASSLBs

With the gradual deepening of research on ASSLBs, developers have realized that interface characteristics have an important impact on the performance of lithium-ion batteries in all respects.[200,201] The common interface types in batteries are solid–liquid and solid–solid. In ASSLBs, the most important is the solid–solid interface, including the cathode–electrolyte interphase film (CEI) and anode solid–electrolyte interphase (SEI) film.[202] Presently, ASSLBs are in the early stage of commercialization, and the problem of interface stability is one of the main bottlenecks restricting their application.[203,204] The solid lithium metal interface problems mainly include:

(1) Mechanical stability: the mechanical stability of the solid electrolyte itself and the mechanical stability of the electrolyte/electrode interface;

(2) Chemical stability: the chemical stability of the interface between solid electrolyte and other electrodes;

(3) Electrochemical stability: the electrochemical stability of the solid electrolytes in a wide potential range;

(4) Thermal stability: the thermal stability of the solid electrolytes and solid electrolyte/electrode interfaces.

The damage caused by interaction of metals with the surrounding environment is called metal corrosion. Metal corrosion occurs at the interface between metal materials and environmental media, and usually includes reactions such as chemical changes, electrochemical changes or physical dissolution. Metals are prone to pitting corrosion,[205,206] intergranular corrosion,[207,208] stress corrosion[209,210] and galvanic corrosion[211,212] in contact with the surrounding environment. Metals are extracted from ores in nature and have a higher free energy, while corrosion is the process by which metals are transformed into metal compounds, the process of returning to their most stable state. In this section, we describe the reaction between lithium metal and solid electrolytes under high voltage from different perspectives, and refer to the concept of metal corrosion and passivation to review and improve electrochemical theory from a new perspective.

4.1 Interfacial problems between high-voltage cathode materials and solid electrolytes

When a high-voltage cathode material is in contact with a solid electrolyte, a co-involved reaction may occur. The solid electrolyte usually has its own stable electrochemical range. When this

Table 4 Interfacial modification of high-voltage ASSLB cathode materials and solid electrolytes

Battery structure (cathode/electrolyte/anode)	Interface modification	Voltage range (V *vs.* Li^+/Li)	Temperature	Capacity [mA h g^{-1}]	Cycle performance	Ref.
LCO + acetylene black + PVDF/LLZO/Li	$LiBO_3$	2.5–4.4 V	RT	67.2 mA h g^{-1}	—	214
LCO + acetylene black + PVDF/PEO/LI	ALD LTO	2.7–4.5 V	60 °C	177 mA h g^{-1}	100	215
LCO + acetylene black + LiBETI: $LiN(SO_2CF_2CF_3)_2$/P(EO/MEEGE/AGE)	Li_3 PO_4	3.0–4.6 V	RT	177 mA h g^{-1}	25	216
LCO + acetylene black + P(EO/MEEGE)-LiBETI/P(EO/MEEGE/AGE)-$LiBF_4$	Al_2O_3	3.0–4.4 V	RT	172 mA h g^{-1}	100	217
LCO + acetylene black + PVDF + PEO/PEO/Li	PECA	2.5–4.45 V	80 °C	175 mA h g^{-1}	75	218
LCO + acetylene black + PVDF/PEO/Li	LATP	2.8–4.5 V	RT	180 mA h g^{-1}	50	219
LCO + acetylene black + PVDF + PEO + LTFSI/PEO/Li	LATP	3.0–4.2 V	60 °C	128 mA h g^{-1}	50	49
NCM622 + acetylene black + PVDF/PEO/Li	APA	2.8–4.3 V	60 °C	190 mA h g^{-1}	80	220
LCO + acetylene black + PVDF/DOL + SN/Li	LiDFOB	2.5–4.3 V	40 °C	138.3 mA h g^{-1}	60	221
NCM_{811} + acetylene black + PVDF/PVDF-HFP + AND + FEC	LiTFSI/ LIBOB	2.8–4.3 V	RT	112 mA h g^{-1}	1000	222
LCO + acetylene black + PVDF + PEO/PEO + LiDFOB/Li	PECA	2.8–4.5 V	30 °C	175 mA h g^{-1}	75	218
NCM622 + acetylene black + PVDF/PEA/Li	PAB	2.5–4.3 V	60 °C	150 mA h g^{-1}	400	223
LCO + acetylene black + PVDF/PEO + LiDFOB/Li	VC	3.0–4.2 V	60 °C	145 mA h g^{-1}	500	224
NCM523 + acetylene black + PVDF/PEO/Li		3.0–4.2 V	60 °C	125 mA h g^{-1}	200	225
LCO + acetylene black + PMA + LiTFSI/PVDF-HFP + PEO/Li	PMA	2.5–4.25 V	65 °C	120 mA h g^{-1}	100	226
NCM111 + acetylene black + PVDF-HFP/PEO/Li	PVDF–HFP	2.5–4.2 V	60 °C	125 mA h g^{-1}	100	227
NCM622 + acetylene black + PVDF + PAN/PEGDA/Li	PAN	2.8–4.3 V	RT	180 mA h g^{-1}	200	90
NCM_{811} + acetylene black + PVDF/PAN + PEO/Li	PAN	2.5–4.3 V	RT	175 mA h g^{-1}	300	228
NCM622 + acetylene black+ PVDF/PAN + LATP + PEO/Li	PAN	2.8–4.3 V	60 °C	158 mA h g^{-1}	120	89
NCM622 + C65 + PPC/PPC + PEO/Li	PPC	2.7–4.2 V	60 °C	155 mA h g^{-1}	80	229
NCM_{811} + acetylene black + PVDF/PAN + PIC + PEO/Li	PAN	2.7–4.3 V	RT	175 mA h g^{-1}	500	230
NCM622 + acetylene black + PAN/PAN + LLAO + PEO + LLZTO/Li	PAN	3.0–4.3 V	30 °C	175 mA h g^{-1}	100	231
NCM_{811} + acetylene black + PVDF/PAN + PEI/graphite electrode	PAN	3.0–4.3 V	RT	200 mA h g^{-1}	200	232
NCM523 + acetylene black + PVDF/PEO/Li	APT	2.8–4.3 V	40 °C	150 mA h g^{-1}	60	87

range is exceeded, it is difficult for the solid electrolyte to remain stable, and it may react with the cathode material.[139] In addition, when the solid electrolyte is in contact with a transition metal with a high oxidation state, the solid electrolyte may undergo an oxidation reaction, transfer electrons to the positive electrode, and even react with the positive electrode material to form an interfacial film covering the surface of the positive electrode material. Co/Ni and lattice oxygen can also intensify the reaction with the solid electrolyte at high-voltage, resulting in their oxidative decomposition.[213] Table 4 summarizes the interfacial modification studies of high-voltage cathode materials and solid electrolytes. Usually, a high-voltage cathode would undergo the following main reactions with a solid electrolyte:

(1) A space charge layer forms due to the different chemical potential of Li^+, which is mainly common in sulfide solid electrolytes and oxide solid electrolytes;

(2) Interdiffusion occurs between the solid electrolyte and the cathode material, which mainly occurs at high temperature or high-voltage, and often forms a new phase of non-Li-ion conductor at the interface;

(3) Oxidative decomposition occurs beyond the electrochemical stability window of the solid electrolyte.

As shown in Fig. 10a, the electrochemical stability window of a PEO solid electrolyte is usually below 4 V, and the LSV curve can be divided into three regions. When the voltage is lower than 3.9 V, the current increases with the applied voltage, which can be attributed to the migration of $TFSI^-$.[233] A significant increase in current can be observed in the voltage range of 3.9–4.5 V, and subsequently it becomes more intense at voltages above 4.5 V. The changes in battery resistance at different potentials were measured using electrochemical impedance spectroscopy (EIS), and the results are shown in Fig. 10b, with little change in interface resistance observable at 4.2 V. When charged to 4.6 V, a violent reaction occurred, and these observations all illustrate the three distinct oxidation stages and final severe oxidation of the PEO–LITFSI solid electrolyte at 4.6 V.[213] Shown in Fig. 10c are the EIS measurements of PEO–LiTFSI batteries in their pristine and 4.6 V state of charge (DC polarization for 48 hours). After 48 hours at 4.6 V, the impedance of the battery dropped significantly due to the severe oxidation of PEO into small molecules. As shown in Fig. 10d and e, when LATP was coated on the surface of $LiCoO_2$, it exhibited better cycling performance than bare $LiCoO_2$, with a capacity retention of 88.6% after 50 cycles. Bare leaked $LiCoO_2$ catalyzed the decomposition of PEO. In contrast, $LiMn_{0.7}Fe_{0.3}PO_4$ batteries showed more stable cycling performance, with a capacity retention rate of 90.3% after 120 cycles.

Research on the interface between a sulfide electrolyte and NCM_{811} by Raimund Koerver[168] showed that when the battery was charged to 3.8 V in the first cycle, the sulfide electrolyte began to undergo oxidative decomposition, resulting in a significant decrease in the first cycle efficiency and an increase in polarization at the same time (Fig. 11b). The charging voltage of $LiCoO_2$ and high-nickel ternary cathodes is usually below 4.6 V. For layered oxides, after the cathode material is deeply delithiated at high voltage, oxygen may participate in charge compensation, resulting in structural instability or even oxygen

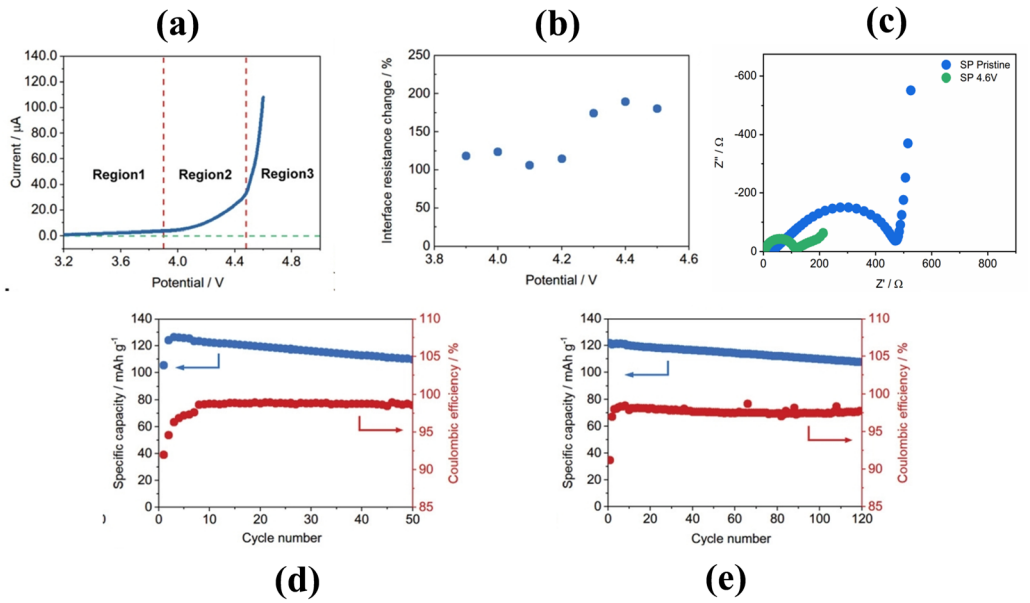

Fig. 10 (a) LSV curve of PEO–LiTFSI batteries at a scanning-rate of 0.1 mV s^{-1} in the voltage range of 3.2–4.6 V. (b) Interfacial resistance change of PEO–LiTFSI batteries at different potentials in comparison with the battery in the initial state. (c) EIS measurements of PEO–LiTFSI batteries in their pristine and 4.6 V charged state (DC polarization for 48 hours). (d) Long cycle performance of LATP coated $LiCoO_2$ and PEO-based solid-state batteries.[213] (e) Long cycle performance of $LiMn_{0.7}Fe_{0.3}PO_4$ and PEO-based solid-state batteries.[213]

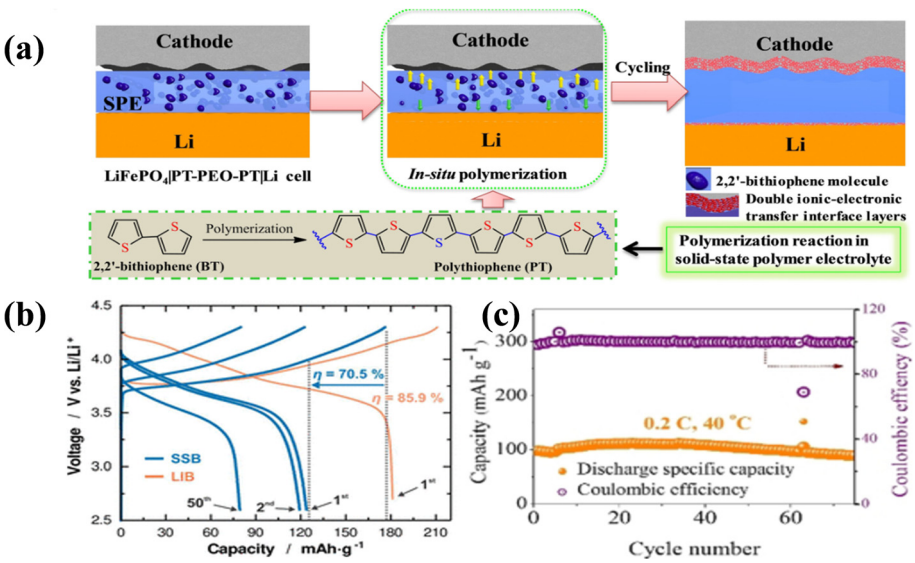

Fig. 11 (a) Electrochemical schematic diagram of the NCM_{523}/PT–PEO–PT/Li battery.[235] (b) Formation of the conductive interface layer in a PEO battery.[168] (c) Long cycle performance of the NCM_{523}/PT–PEO–PT/Li battery at 40 °C.[235]

production. For spinel-type cathodes, although the generation energy of oxygen vacancies is positive, there is still a certain probability of generating oxygen vacancies. Especially for the positive electrode material in the charged state, the transition metal on the surface is in a high-valence state and has strong oxidizing ability, which makes it easier to oxidize and decompose the solid electrolyte. CEI films are generally unstable at high voltage, with an increase in CEI in the charged state and a decrease after discharge. This is because Li^+ intercalates into and diffuses in the CEI film, resulting in partial exfoliation of the CEI film.[234] As shown in Fig. 11a and c, in order to reduce the influence of the CEI film on a solid electrolyte, Zheng[235] used electrochemical polymerization to improve the solid electrolyte cathode interface (CEI), and tested it with NCM_{523}, showing a fairly stable long cycle performance.

4.2 Interfacial problems between a solid electrolyte and lithium metal

The anode realizes the reversible insertion and removal of lithium ions in the battery, and plays a decisive role in

improving the performance of lithium ion batteries. At present, the commonly used anode materials include lithium metal anode materials, carbon based anode materials, silicon based anode materials, tin based anode materials and so on. The lithium metal anode has attracted extensive attention due to its ultra-high theoretical specific capacity (3860 mA h g^{-1}), lowest standard electrode position (−3.040) and lowest density (0.534 g cm^{-3}). Therefore, lithium metal can react with any electrolyte immediately.[236] The industrial application of lithium metal is hindered by factors such as lithium loss and lithium dendrites.[237] In the absence of any externally applied current or electrode potential, due to the unstable interface chemistry, when the solid electrolyte is in contact with the lithium metal, the lithium metal corrodes or passivates to form an uncontrollable solid electrolyte interfacial film (SEI). Whether the film is conducive to the migration of Li^+ or not can affect the charge and discharge performance of the battery to a certain extent. Current research on lithium metal mainly focuses on surface modification to improve its reversibility, morphological stability and rate capability.[238–240] In addition, researchers have also carried out a lot of research on the interface problem between lithium metal and solid electrolytes. Wang[241] used molten lithium and AlF_3 to form a functional gradient lithium anode (FGLA) by self regulating reaction. The reaction of molten lithium and AlF_3 spontaneously formed a composition gradient of Li–LiAl–LiF, in which LiAl reduced the interface resistance, and LiF was used to inhibit Li dendrites. The all-solid-state battery composed of the NCM_{523} high-voltage cathode material and LLZTO solid electrolyte showed excellent cycle stability. Wu[242] compounded lithium metal and ferromagnetic particles into an engineered metal lithium. The magnetic effect of iron caused the lithium metal to contact LLZTO closely, and the interface resistance decreased significantly. The solid-state battery assembled with a $LiFePO_4$ cathode material exhibited excellent cycling performance. However, most studies ignore the fact that lithium is a metal, and metal is easily corroded in contact with the surrounding environment to form a passivation film that covers the metal surface. Its composition, thickness, morphology and uniformity have an important impact on the performance of the battery.[243–247] Becking[243] showed that the mechanical flattening and thinning of the natural passivation layer on Li metal is beneficial to the improvement of battery cycling stability. Etxebarra's studies showed limited reproducibility in purchasing lithium metal of similar purity from different buyers, with measured capacity variations of up to 7%.[248] Therefore, controllable pre-passivation and functionalization of Li metal anode surfaces are necessary.

In general, atmospheric gases such as N_2, O_2, H_2O and CO_2 are the main residues in an argon atmosphere in the glove box, and they are the main components that come into contact with lithium metal during storage and processing. The reaction of lithium to atmospheric gases was reported in the 1960s.[249–255] These reports generally mention the high reactivity of lithium metal with water, but the results on the reactivity with other atmospheric gases are quite contradictory, which may be caused by different research environments. A high reaction rate of the lithium surface with oxygen has been reported by some researchers.[256,257] However, others ignore the reaction between lithium and oxygen, and even treat oxygen as a noble gas.[249,250] Several recent publications discuss and attempt to explain these contradictions, but do not fully answer unresolved questions such as the intrinsic reactivity of nitrogen and lithium.[248,258]

The corrosion or passivation film formation of Li is shown in Fig. 12 and can be described by two electrochemical reactions, which are parallel and at the same rate:

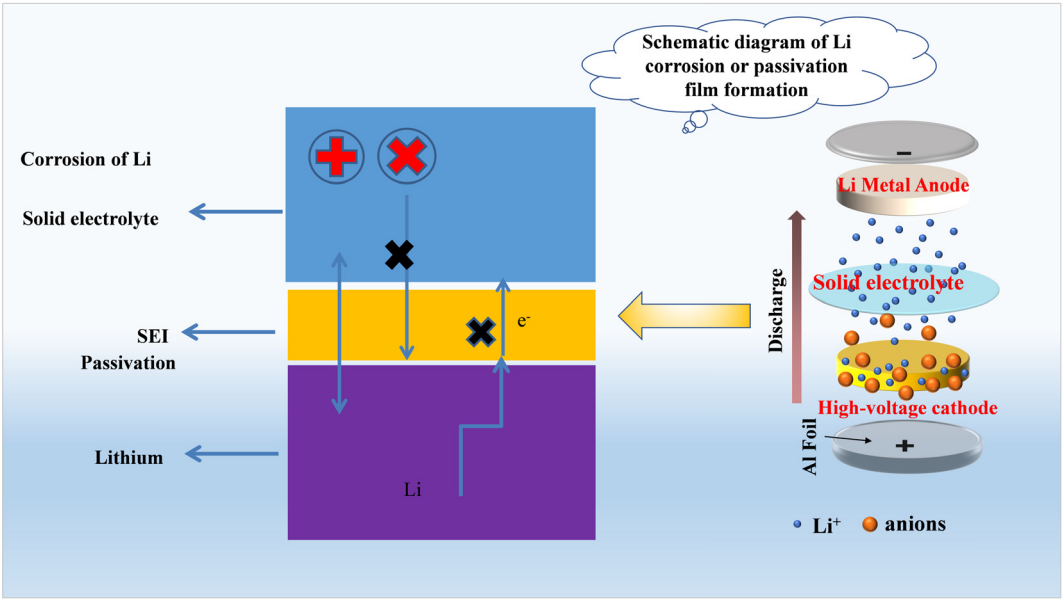

Fig. 12 Schematic diagram of Li corrosion or passivation film formation.

The anode partial reaction eqn (1) includes Li oxidation or dissolution:

$$n\mathrm{Li} \rightarrow n\mathrm{Li}^{+} + n\mathrm{e}^{-} \quad (1)$$

The cathode partial reaction eqn (2) includes electrolyte reduction:

$$\text{Electrolyte} + n\mathrm{e}^{-} \rightarrow \text{SEI} + \text{soluble species} + \text{gaseous species} \quad (2)$$

Lithium corrosion or passivation film formation involves different kinds of solid electrolytes, and the various chemical and electrochemical reactions that occur are also different. These reactions occur simultaneously and interfere with each other. The composition of the SEI film formed by these reactions is complex (depending on the type of solid state of the electrolyte). As shown in Fig. 13, in general, corrosion and passivation film formation can be divided into three stages (analysis was taken from ref. 259.

All corrosion and passivation processes are assumed to occur spontaneously, immediately upon contact with the solid electrolyte. In addition, in the case of external high temperature and high voltage, the solid electrolyte can also change during the charging and discharging process of the battery, thereby affecting the interface behavior.

Corrosion behavior occurrs when Li is in contact with the solid electrolyte for a few picoseconds, and even the thickness of the SEI film formed only at the nanoscale (stage 1) results in considerable changes in performance. The growth of the surface film prevents the diffusion of the solid electrolyte to the Li metal surface through the formation of a charge transfer barrier, protecting the Li metal from the solid electrolyte. In general, the corrosion rate (R_M) can be derived as a function of the corrosion current i_{corr}, as shown in eqn (3):

$$R_M = \frac{M}{nFP} i_{corr} \quad (3)$$

where M is the molar mass of the metal, ρ is its density, n is the number of charges, representing the number of electrons exchanged, and F is the Faraday constant (96 485 C mol^{-1}), which can be derived from the corrosion current density i_{corr} of the circuit, as in formula (4):

$$i_{corr} = FS[k_c CO(0,t) - k_a C_R(0,t)] \quad (4)$$

where k_c is the cathodic reaction rate constant, C_0 is the concentration of oxidizing species, k_a is the anodic reaction rate constant, C_R is the concentration of reducing species, and S is the electrode surface area in contact with the solid electrolyte.

As shown in formula (5), according to the Arrhenius equation, the reaction rate constant K is related to the Arrhenius constant A (for a specific element), the activation energy E_a of the corrosion process (including the activation energy and the large contribution of the electric field), usual gas constant R (8.314 J mol^{-1} K^{-1}) and absolute temperature T (TETS):

$$K = Ae^{-E_a/RT} \quad (5)$$

At open circuit voltage, reactions proceed according to eqn (1) and (2). The open-circuit voltage potential, the corrosion potential (E_c), is a mixed potential that represents the polarization of the surface lithium oxidation sites and the solid-state electrolyte reduction sites. Therefore, the reaction rate K can be expressed as:

$$K = k_0 \exp\left[\frac{E_{\text{Electrolyte}^0} - E_C}{RT/\alpha nF}\right] \quad (6)$$

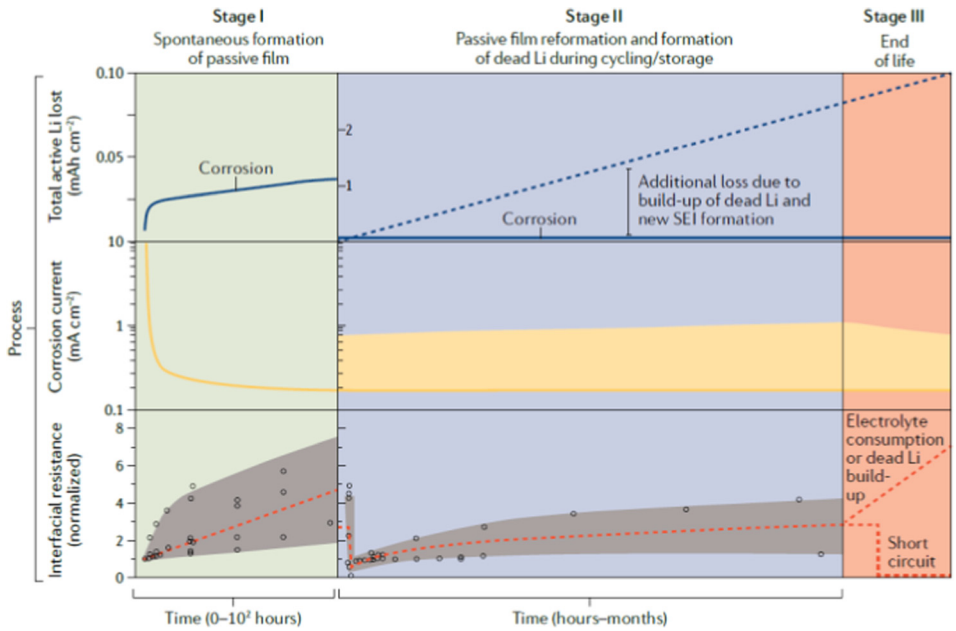

Fig. 13 Schematic diagram of corrosion of lithium in nonaqueous electrolytes, including ether-based or organic carbonate based electrolytes.[259]

where k_0 is the rate constant at $E = E_{\text{Electrolyte}^0}$, α is the transfer coefficient, and the term $E = E_{\text{Electrolyte}^0} - E_c$ represents the local cell potential of the lithium oxidation and electrolyte reduction pair. Due to the formation of (lithium-containing) electrolyte decomposition products at the interface, the corrosion potential of Li in the electrolyte decreases significantly for a short time, and thus the reaction rate decreases. In fact, the charge transfer from the electrode to the electrolyte or electrolyte reduction intermediate becomes so slow that the evolution current drops by orders of magnitude to a negligible current. At this point, the lithium corrosion rate is the lowest.

As shown in formula (7), the thickness $S(t)$ of the passivation film (SEI film) can theoretically be deduced from the total moles of Li involved in the SEI to form NS (given each surface area), the molar mass of the SEI component M, their density ρ and the amount of Li per component n.

$$S(t) = \frac{M}{np} N_{\text{SEI}}(t) \tag{7}$$

Under the condition that the passivation film is formed spontaneously and a high voltage is applied externally, further electron transfer occurs in the battery during cycling. Considering the extremely low redox potential of Li metal, the electromotive force generated by external polarization (tens of millivolts) of the SEI or solid-state electrolyte decomposition is negligible. Nonetheless, the polarization of lithium metal may facilitate additional reactions in the SEI film through electron tunneling and migration of electroactive species. Svenia-K[260] chose LLZO, which is very stable for lithium, and investigated lithium corrosion/passivation film formation. Although some researchers have reported interfacial reactions between LLZO and lithium metal, these interfacial reactions are need not be considered.

As shown in Fig. 14, Svenia-K[260] investigated the effect of glovebox storage conditions on the passivation films of commercial lithium foils, and the effect of the passivation film on the interfacial resistance when the lithium foil is used as the anode. A rough solid electrolyte can significantly reduce the interfacial resistance because the solid electrolyte would penetrate the passivation film. Reaction tests of lithium metal with dry N_2, O_2, and CO_2 and wet Ar indicated that the reaction with residual water may be the main factor for the growth of the passivation films. In conclusion, storage conditions and reation conditions are important factors affecting the surface impedance of Li metal, they need to be considered in battery applications, and this reaction stage mainly occurs in stage one.

At present, the observed reaction and SEI evolution are mainly driven by morphological changes induced by Li metal exfoliation and electroplating from the anode (depending on the corresponding active material on the cathode) (stage two). The reaction in stage one is low in selectivity and usually spontaneous. However, stage two is mainly an electrochemical process with high selectivity. The initial formation of the passivation layer (stage one) involved in the electrochemical

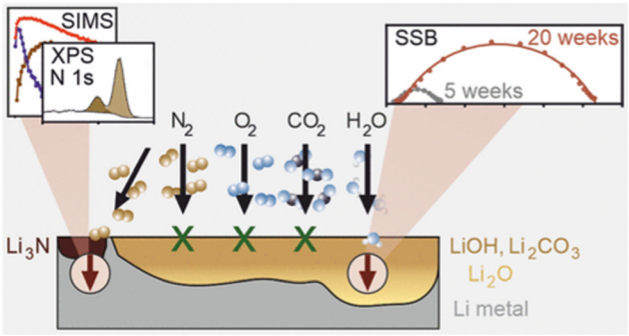

Fig. 14 Diagram of the reaction interface between Li and different substances.[260]

reaction process, the solid electrolyte got electrons, lithium deforms, and the solid electrolyte also participated in the reaction. The products formed were piled up with each other, and the composition was complex. Different from the composition of the passivation layer, the passivation layer collapsed due to Li depletion (possibly in the form of pores and voids). In the case of electroplating lithium, due to the unevenness of the electroplating, which leads to the formation of lithium dendrites, the film breaks down, exposing the surface of fresh lithium to the electrolyte and the outer passivation film of the electrode. In addition, electron tunneling in the portion of the SEI film adjacent to the electrode may lead to intralayer transition of lithium, which further changes the composition of the surface film. In any case, these electrochemical reactions induce mechanical stress between the surface film and the Li surface, and lead to localized striking of the film and exposure of fresh lithium. In a sense, the instantaneous reaction of this solid electrolyte, along with the evolution of the high-surface–area lithium structure and the continuous emergence of local fresh surfaces, can be considered as a self-healing local repassivation process. The generation of cracks is caused by the lattice mismatch of Li_2O and LiO. Passivation films of lithium metal in solid electrolytes are not good for batteries because such films are not fully electrically insulating. This process can be described by eqn (8). The potential distributions that generate the cracks and the current and potential distributions at the outer surface have been numerically solved, using the Butler–Volmer equation to calculate the reduction of the electrolytically dissolved passivation surface of the metal and electrolyte at the crack tip as boundary conditions.

$$\int_s i_c d_s = -i_{\text{crack}} A_{\text{crack}} \tag{8}$$

where i_{crack} is the current density at the crack opening, the area is A_{crack}, i_c is the current density corresponding to the solid electrolyte on the outer surface, and d_s is the increment of the area exposed to the solid electrolyte. The electrons present at the interface of the solid-state electrolyte participate in the formation of the SEI film with non-uniform thickness and combine with the products of electrolyte decomposition to form so-called "dead lithium", which is also the main reason

for the loss of coulombic efficiency (CE). The interfacial resistance of ion diffusion changes over the lifetime and eventually decreases due to increased surface area (caused by morphological changes) and eventually corrosion and electrolyte decomposition products increase at the interface.

The lithium corrosion and repassivation process eventually leads to battery failure (stage three), which is not related to corrosion, either the formation of lithium dendrites short-circuits the battery or the electrochemical reaction allows the lithium to be completely consumed. The first two processes cause the battery to short out and fail. However, a short circuit presents a problem as it causes a rapid release of heat and eventually a thermal runaway of the battery, which is a serious safety concern in terms of fire or explosion hazards. Therefore, a comprehensive understanding of the mechanisms of the interfacial processes and chemical reactions that take place in the first and second stages is crucial to solving the problems related to stage three.

At present, lithium metal and the metal collector are combined to form a composite anode to mitigate lithium dendrite formation.[261] When the composite cathode contacts with the solid electrolyte, the two metals are prone to galvanic corrosion due to their different corrosion potentials. Galvanic corrosion usually occurs spontaneously and lithium usually is the corroded side due to the strong activity of lithium, which changes the morphology of lithium metal and produces a more severe lithium dendrite effect. Galvanic corrosion usually requires four links: cathode, anode, electrolyte and conductor. If one link disappears, galvanic corrosion would not occur. Modification of the metal collector can alleviate the lithium dendrite problem. It should be noted that galvanic corrosion of the metal collector and lithium metal causes a change of lithium metal morphology.

4.3 Solving of solid state battery interface problems

Interface problems have an important impact on the performance of batteries. Therefore, it is very important to solve the interface problems of batteries. The following aspects should be paid more attention in interface problem research on ASSLBs.

(1) The research on interface problems of traditional ASSLBs should be further strengthened;

(2) New high-voltage solid electrolytes should be developed with better compatibility with positive and negative electrode materials;

(3) More attention should be paid to the corrosion phenomenon of interface problems in ASSLBs.

5. Insights into the failure behavior of ASSLBs

With the development of solid-state battery research, ASSLBs with excellent performance have been developed. However, the failure mechanism of ASSLBs is not understood. The failure behavior of ASSLBs can reduce the energy density and power density of the battery, and have a significant impact on the reliability, safety and cycle life of the battery. It is necessary to fully understand the failure mechanism of all solid-state batteries in order to build safe batteries. The failure of ASSLBs is affected by many factors, such as electrode material, electrolyte type and environment. The interface reaction between electrode and electrolyte, as well as the growth of lithium dendrites on the anode may cause the failure of ASSLBs. In recent years, some researchers have studied the failure of solid-state batteries. Wen's[262] research showed that the voltage attenuation of Li-and Mn-rich layered cathode materials was caused by a layered-to-spinel phase change in the bulk, and the serious reduction of particle surface played a key role, indicating that the type of electrode materials had an important impact on the failure of ASSLBs. Huang[263] studied the interphase degradation of a 4.2 V-class poly(ethylene oxide)-based solid battery beyond the electrochemical voltage limit. It was found that the mismatch between PEO electrolyte and 4 V-class cathode was not only due to the limited electrochemical window of PEO electrolyte, but also to the serious surface reconstruction and well aligned nano voids observed on most of the failed NCM surfaces. Liu[264] comprehensively summarized the failure mechanism of ASSLBs, and understanding the basic failure mechanism provided an important scientific basis for building an efficient ASSLB.

6. Challenges and outlook

This review summarizes high-voltage cathode materials, solid-state electrolytes and interfacial issues between solid-state electrolytes and cathodes and anodes. In the future, there will be a great demand for lithium metal batteries with a long cycle life and high energy density. As the improvement of energy density of liquid batteries is approaching the limit, ASSLBs will be the focus of lithium metal battery research. High voltage solid electrolytes are the key to building ASSLBs with a long cycle life and high energy density, and they are also the focus of ASSLB research, which has a significant impact on the commercialization of ASSLBs. With the development of technology, high-voltage solid electrolytes should make great progress. However, there are still few studies on high-voltage solid electrolytes, which are still in their infancy and still face many challenges. The currently available high-voltage solid electrolytes cannot meet the requirements of commercialization. First, solid electrolytes require a wider electrochemical window. Second, high-voltage cathode materials in a highly delithiated state exhibit strong oxidation activity, which accelerates the decomposition of solid-state electrolytes, and high-voltage cathode materials must be highly compatible with solid-state electrolytes. Third, the solid electrolyte needs to match the thick high-voltage cathode material, so that the solid electrolyte has better energy density than the liquid electrolyte, and finally the interface problem between the solid electrolyte and the positive/negative electrodes needs to be overcome. Fig. 15 summarizes some of the problems faced by high-voltage solid-state electrolytes and their corresponding solutions.

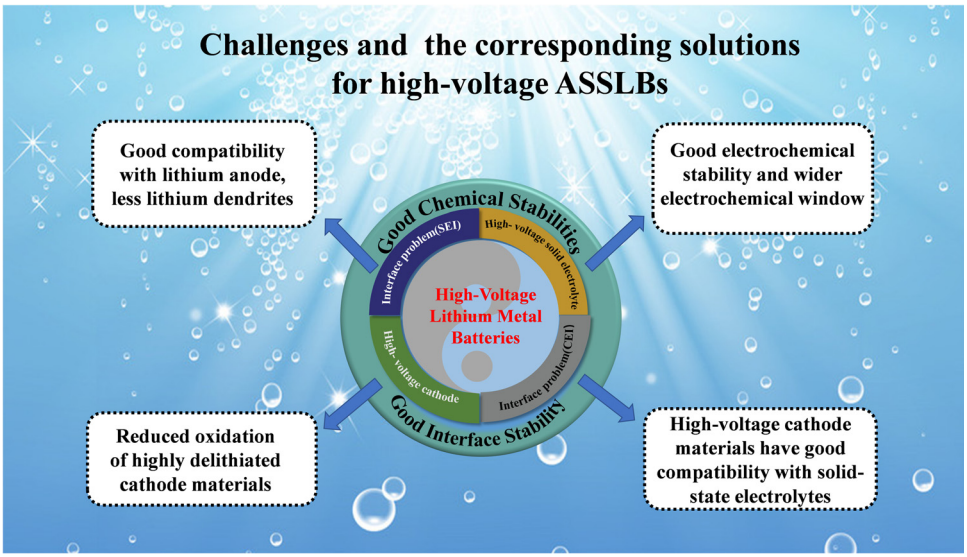

Fig. 15 Schematic illustration of the challenges and corresponding solutions for assembling high-voltage high-performance ASSLBs.

According to our observations, high-voltage solid-state electrolytes should develop in the following directions:

(1) The high-voltage performance of the commonly used high-voltage solid electrolytes is generally unsatisfactory, and the modification of high-voltage solid electrolytes is still the focus of future research;

(2) At present, high-voltage solid electrolytes have poor compatibility with different high-voltage cathode materials, and improving the compatibility of solid-state electrolytes with different high-voltage cathode materials is one of the key research priorities for the future;

(3) The coating of high-voltage cathode materials can effectively suppress interfacial side reactions. By coating the precursor of the cathode material, the structural transformation of the high-voltage cathode material at high voltage, the release of lattice oxygen, and the occurrence of interfacial side reactions can be suppressed;

(4) Reaction tests of Li foil with dry N_2, O_2, and CO_2 and wet Ar indicated that the reaction with residual water may be the main factor for the growth of Li metal passivation films. Storage conditions and reaction conditions are important factors affecting the surface impedance of lithium foils and need to be considered in battery applications.

Author contributions

Mingming Ma: investigation, writing – original draft. Menghui Zhang: visualization. Bitao Jiang: data curation. Yang Du: formal analysis. Bingcheng Hu: resources, project administration, supervision. Chengguo Sun: writing – review & editing, validation.

Conflicts of interest

The authors declare no conflict of interest.

Acknowledgements

The authors thank the National Natural Science Foundation of China (No. 21975128 and 11972178).

References

1 Y. Zhu, S. Zhou, Y. Feng, Z. Hu and L. Yuan, Influences of solar energy on the energy efficiency design index for new building ships, *Int. J. Hydrogen Energy*, 2017, **42**(30), 19389–19394.

2 M. Younas and M. Gondal, Economical and efficient dye sensitized solar cells using single wall carbon nanotube-titanium dioxide nanocomposites as photoanode and SWCNT as Pt-free counter electrode, *Sol. Energy*, 2022, **245**, 37–45.

3 D. Xia, W. Xuan, X. Nairui, T. Yehua, P. Chengxiao and W. Ke-Fan, Atomic structure, electronic structure and optical absorption of inorganic perovskite compounds Cs_2SnI_6-nX_n (X = F, Cl, br; n = 0–6): a first-principles study, *Sol. Energy*, 2022, **245**, 25–36.

4 M. Shoaib, I. Siddiqui, S. Rehman, S. Khan and L. M. Alhems, Assessment of wind energy potential using wind energy conversion system, *J. Cleaner Prod.*, 2019, **216**, 346–360.

5 A. Dupré, P. Drobinski, B. Alonzo, J. Badosa, C. Briard and R. Plougonven, Sub-hourly forecasting of wind speed and wind energy, *Renewable Energy*, 2020, **145**, 2373–2379.

6 C. Liu, M.-S. Cheng, B.-C. Zhao and Z.-M. Dai, A wind power plant with thermal energy storage for improving the utilization of wind energy, *Energies*, 2017, **10**(12), 2126.

7 M. Aliehyaei, R. Kumar, A. Ahmadi and D. H. Jamali, Energy, exergy and economic analyses of new coal-fired cogeneration hybrid plant with wind energy resource, *J. Cleaner Prod.*, 2020, **269**, 122331.

8 M. B. Topper, V. Nava, A. J. Collin, D. Bould, F. Ferri, S. S. Olson, A. R. Dallman, J. D. Roberts, P. Ruiz-Minguela and H. F. Jeffrey, Reducing variability in the cost of energy of ocean energy arrays, *Renewable Sustainable Energy Rev.*, 2019, **112**, 263–279.
9 N. Viet, X. Xie, K. Liew, N. Banthia and Q. Wang, Energy harvesting from ocean waves by a floating energy harvester, *Energy*, 2016, **112**, 1219–1226.
10 E. S. Pampal, E. Stojanovska, B. Simon and A. Kilic, A review of nanofibrous structures in lithium ion batteries, *J. Power Sources*, 2015, **300**, 199–215.
11 H. Wang, H. Gao, X. Chen, J. Zhu, W. Li, Z. Gong, Y. Li, M. S. Wang and Y. Yang, Linking the Defects to the Formation and Growth of Li Dendrite in All-Solid-State Batteries, *Adv. Energy Mater*, 2021, **11**(42), 2102148.
12 J. Li, C. Ma, M. Chi, C. Liang and N. J. Dudney, Solid Electrolyte: The Key for High-Voltage Lithium Batteries, *Adv. Energy Mater.*, 2015, **5**(4), 1401408.
13 M. Ogawa, R. Kanda, K. Yoshida, T. Uemura and K. Harada, High-capacity thin film lithium batteries with sulfide solid electrolytes, *J. Power Sources*, 2012, **205**, 487–490.
14 Y. Zheng, Y. Yao, J. Ou, M. Li, D. Luo, H. Dou, Z. Li, K. Amine, A. Yu and Z. Chen, A review of composite solid-state electrolytes for lithium batteries: fundamentals, key materials and advanced structures, *Chem. Soc. Rev.*, 2020, **49**(23), 8790–8839.
15 K. H. Kim and S. H. Hong, Manganese Tetraphosphide (MnP_4) as a High Capacity Anode for Lithium-Ion and Sodium-Ion Batteries, *Adv. Energy Mater.*, 2021, **11**(9), 2003609.
16 N. V. Aspern, S. R. Ser, B. R. Rad, P. Murmann, B. Streipert, X. M. Nnighoff, S. D. Tillmann, M. Shevchuk, O. Stubbmann-Kazakova and G. V. R. Schenthaler, Phosphorus additives for improving high voltage stability and safety of lithium ion batteries, *J. Fluorine Chem.*, 2017, **198**, 24–33.
17 J. I. Lee, M. Shin, D. Hong and S. Park, Efficient Li-Ion-Conductive Layer for the Realization of Highly Stable High-Voltage and High-Capacity Lithium Metal Batteries, *Adv. Energy Mater.*, 2019, **9**(13), 1803722.
18 M. Yao, Q. Ruan, T. Yu, H. Zhang and S. Zhang, Solid polymer electrolyte with in situ generated fast Li^+ conducting network enable high voltage and dendrite-free lithium metal battery, *Energy Storage Mater.*, 2022, **44**, 93–103.
19 Y. N. Yang, F. L. Jiang, Y. Q. Li, Z. X. Wang and T. Zhang, Surface Coordination Interphase Stabilizes Solid state Battery, *Angew. Chem., Int. Ed.*, 2021, **60**, 2–11.
20 H. Sun, X. Xie and Q. Huang, *et al.*, Fluorinated Polyoxalate Electrolytes Stabilizing both Anode and Cathode Interfaces for All-Solid-State Li/NMC811 Batteries, *Angew. Chem.*, 2021, **133**(33), 18483–18491.
21 T. Takahashi, Early History of Solid State Ionics, *MRS Online Proc. Libr.*, 1988, **135**(7), 599.
22 G. Wiedemann, Die Lehre von der Elektricitat, F. Vieweg and Braunschweig, *The Science of Electricity*, 2nd edn, 1893.
23 T. Takahashi and O. Yamamoto, The $Ag/Ag_3SI/I_2$ solid–electrolyte cell, *Electrochim. Acta*, 1966, **11**(7), 779–789.
24 Y. Yung-Fang Yu and J. T. Kummer, Ion exchange properties of and rates of ionic diffusion in beta-alumina, *J. Inorg. Nucl. Chem.*, 1967, **29**(9), 2453–2475.
25 D. Fenton, Complexes of alkali metal ions with poly(ethylene oxide), *Polymer*, 1973, **14**, 589.
26 M. B. Armand, J. M. Chabagno and M. Duclot, *Fast ion transport in solids electrodes and electrolytes conference*, 1979, **131**.
27 J. Coetzer, A new high energy density battery system, *J. Power Sources*, 1986, **18**(4), 377–380.
28 R. J. Bones, J. Coetzer and R. C. Galloway, *et al.*, A sodium/iron(II) chloride cell with a beta alumina electrolyte, *J. Electrochem. Soc.*, 1987, **134**(10), 2379–2382.
29 N. Dudney, J. Bates, R. Zuhr, C. Luck and J. Robertson, Sputtering of lithium compounds for preparation of electrolyte thin films, *Solid State Ionics*, 1992, **53**, 655–661.
30 K. Onishi, M. Matsumoto and K. Shigehara, Lithium batteries composed of aluminate polymer complexes as single-ion conductive solid electrolytes, *J. Power Sources*, 2001, **92**(1–2), 120–123.
31 T. Venkataraman, K. Heiko, J. Werner and F. Weppner, Novel Fast Lithium Ion Conduction in Garnet-Type $Li_5La_3M_2O_{12}$ (M = Nb, Ta), *J. Am. Ceram. Soc.*, 2003, **86**(3), 437–440.
32 C. Escher, T. Latychevskaia, H. W. Fink and D. W. Pohl, Direct Evidence for Conduction Pathways in a Solid Electrolyte, *Phys. Rev. Lett.*, 2006, **97**(13), 136601.
33 N. Kamaya, K. Homma, Y. Yamakawa, M. Hirayama, R. Kanno, M. Yonemura, T. Kamiyama, Y. Kato, S. Hama and K. Kawamoto, A lithium superionic conductor, *Nat. Mater.*, 2011, **10**(9), 682–686.
34 J. K. Kim, J. Scheers, T. J. Park and Y. Kim, Superior Ion-Conducting Hybrid Solid Electrolyte for All-Solid-State Batteries, *ChemSusChem*, 2015, **8**(4), 636–641.
35 L. Zhou, T. T. Zuo, C. Y. Kwok, S. Y. Kim, A. Assoud, Q. Zhang, J. Janek and L. F. Nazar, High areal capacity, long cycle life 4 V ceramic all-solid-state Li-ion batteries enabled by chloride solid electrolytes, *Nat. Energy*, 2022, **7**(1), 83–93.
36 S. Ahmed, P. A. Nelson, K. G. Gallagher, N. Susarla and D. W. Dees, Cost and energy demand of producing nickel manganese cobalt cathode material for lithium ion batteries, *J. Power Sources*, 2017, **342**, 733–740.
37 R. K. Katiyar, R. Singhal, K. Asmar, R. Valentin and R. S. Katiyar, High voltage spinel cathode materials for high energy density and high rate capability Li ion rechargeable batteries, *J. Power Sources*, 2009, **194**(1), 526–530.
38 S. Kalluri, M. Yoon, M. Jo, S. Park, S. Myeong, J. Kim, S. X. Dou, Z. Guo and J. Cho, Surface Engineering Strategies of Layered $LiCoO_2$ Cathode Material to Realize High-Energy and High-Voltage Li-Ion Cells, *Adv. Energy Mater.*, 2017, **7**(1), 1601507.
39 S. Li, K. Zhu, D. Zhao, Q. Zhao and N. Zhang, Porous $LiMn_2O_4$ with Al_2O_3 coating as high-performance positive materials, *Ionics*, 2018, **25**, 1991–1998.

40 Y. Huang, Mg-pillared $LiCoO_2$: Towards Stable Cycling at 4.6 V, *Angew. Chemie*, 2020, **133**(9), 4732–4738.
41 W. Zeng, Q. Chen, Y. Li, C. Chen, X. Liu, M. Yuan, R. Wang, S. Chen and S. Xiao, Enhanced electrochemical performances of $LiNi_{0.8}Co_{0.1}Mn_{0.1}O_2$ by synergistic modification of sodium ion doping and silica coating, *Solid State Ionics*, 2020, **346**, 115214.
42 X. Z. Kong, D. L. Li, K. Lahtinen, T. Kallio and X. Q. Ren, Effect of Copper-Doping on $LiNiO_2$ Positive Electrode for Lithium-Ion Batteries, *J. Electrochem. Soc.*, 2020, **167**(14), 140545.
43 X. Zhang, G. Liu, S. Li, H. Dong, H. Liu and J. Mei, Preparation of a Homogeneous Li_3PO_4 Coating and Its Effect on the Electrochemical Properties of $LiNi_{0.8}Co_{0.15}Al_{0.05}O_2$, *J. Electron. Mater.*, 2019, **48**, 4443–4451.
44 N. Kosova, O. Podgornova, I. Bobrikov, V. Kaichev and A. Bukhtiyarov, Approaching better cycleability of $LiCoPO_4$ by vanadium modification, *Mater. Sci. Eng., B*, 2016, **213**, 105–113.
45 S. Karthickprabhu, D. Vikraman, A. Kathalingam, K. Prasanna, H.-S. Kim and K. Karuppasamy, Electrochemical and cycling performance of neodymium (Nd^{3+}) doped $LiNiPO_4$ cathode materials for high voltage lithium-ion batteries, *Mater. Lett.*, 2019, **237**, 224–227.
46 J.-J. Pan, B. Chen, Y. Xie, N. Ren and T.-F. Yi, V_2O_5 modified $LiNi_{0.5}Mn_{1.5}O_4$ as cathode material for high-performance Li-ion battery, *Mater. Lett.*, 2019, **253**, 136–139.
47 E. D. Jeong, M. S. Won and Y. B. Shim, Cathodic properties of a lithium-ion secondary battery using $LiCoO_2$ prepared by a complex formation reaction, *J. Power Sources*, 1998, **70**(1), 70–77.
48 J. Wang, Z. Liang, Y. Zhao, J. Sheng, J. Ma, K. Jia, B. Li, G. Zhou and H.-M. Cheng, Direct Conversion of Degraded $LiCoO_2$ Cathode Materials into High-Performance $LiCoO_2$: A Closed-Loop Green Recycling Strategy for Spent Lithium-Ion Batteries, *Energy Storage Mater.*, 2022, **45**, 768–776.
49 J. Qiu, X. Liu, R. Chen, Q. Li, Y. Wang, P. Chen, L. Gan, S. J. Lee, D. Nordlund and Y. Liu, Enabling stable cycling of 4.2 V high-voltage all-solid-state batteries with PEO-based solid electrolyte, *Adv. Funct. Mater.*, 2020, **30**(22), 1909392.
50 Z. Lv, Q. Zhou, S. Zhang, S. Dong, Q. Wang, L. Huang, K. Chen and G. Cui, Cyano-reinforced in situ polymer electrolyte enabling long-life cycling for high-voltage lithium metal batteries, *Energy Storage Mater.*, 2021, **37**, 215–223.
51 C. Wang, H. Zhang, S. Dong, Z. Hu, R. Hu, Z. Guo, T. Wang, G. Cui and L. Chen, High polymerization conversion and stable high-voltage chemistry underpinning an in situ formed solid electrolyte, *Chem. Mater.*, 2020, **32**(21), 9167–9175.
52 H. Wu, B. Tang, X. Du, J. Zhang, X. Yu, Y. Wang, J. Ma, Q. Zhou, J. Zhao and S. Dong, LiDFOB initiated in situ polymerization of novel eutectic solution enables room-temperature solid lithium metal batteries, *Adv. Sci.*, 2020, **7**(23), 2003370.
53 Z. Wang, L. Shen, S. Deng, P. Cui and X. Yao, 10 μm-Thick High-Strength Solid Polymer Electrolytes with Excellent Interface Compatibility for Flexible All-Solid-State Lithium-Metal Batteries, *Adv. Mater.*, 2021, **33**(25), 2100353.
54 J. Yu, Z. Han, X. Hu, H. Zhan, Y. Zhou and X. Liu, Solid-state synthesis of $LiCoO_2$/$LiCo_{0.99}Ti_{0.01}O_2$ composite as cathode material for lithium ion batteries, *J. Power Sources*, 2013, **225**, 34–39.
55 A. Qz, A. Hx, L. A. Lu, A. Wl, L. A. Yan, B. Hl and C. Tong, Study on the decline mechanism of cathode material $LiCoO_2$ for Li-ion battery, *Vacuum*, 2020, **177**, 109313.
56 I. Ilahi, A. M. Yousafzai, M. Attaullah, T. U. Haq, A. Rahim, W. Khan, A. A. Khan, S. Ullah, T. Jan and M. M. Khan, Mosquitocidal activities of Chenopodium botrys whole plant *n*-hexane extract against Culex quinquefasciatus, *Braz. J. Biol.*, 2021, **83**, e240842.
57 C. Marianetti, A. Kotliar and G. Ceder, A first-order Mott transition in Li_xCoO_2, *Nat. Mater.*, 2004, **3**(9), 627–631.
58 J. N. Reimers and J. R. Dahn, Electrochemical and Insitu X-Ray-Diffraction Studies of Lithium Intercalation in Li_xCoO_2, *J. Electrochem. Soc.*, 1992, **139**(8), 2091–2097.
59 Z. Chen, Z. Lu and J. Dahn, Staging phase transitions in Li_xCoO_2, *J. Electrochem. Soc.*, 2002, **149**(12), A1604.
60 A. V. D. Ven, M. K. Aydinol and G. Ceder, First-principles evidence for stage ordering in Li_xCoO_2, *J. Electrochem. Soc.*, 1998, **145**(6), 2149–2155.
61 G. G. Aamatucci, J. M. Tarascon and L. C. Klein, CoO_2, the end member of the $LixCoO_2$ solid solution, *J. Electrochem. Soc.*, 1996, **143**(3), 1114.
62 C. M. Julien, A. Mauger, K. Zaghib and H. Groult, Comparative issues of cathode materials for Li-ion batteries, *Inorganics*, 2014, **2**(1), 132–154.
63 Q. Zhou, H. Xu, W. Liu, Y. Liang, H. Li and T. Chen, Study on the decline mechanism of cathode material $LiCoO_2$ for Li-ion battery, *Vacuum*, 2020, **177**, 109313.
64 H. Xia, S. Y. Meng, L. Lu and G. Ceder, Electrochemical Behavior and Li Diffusion Study of $LiCoO_2$ Thin Film Electrodes Prepared by PLD, 2007, **https://hdl.handle.net/1721.1/35827**.
65 G. Amatucci, J. Tarascon and L. Klein, CoO_2, the end member of the Li_xCoO_2 solid solution, *J. Electrochem. Soc.*, 1996, **143**(3), 1114.
66 W. Kong, J. Zhang, D. Wong, W. Yang, J. Yang, C. Schulz and X. Liu, Tailoring Co 3d and O 2p Band Centers to Inhibit Oxygen Escape for Stable 4.6 V $LiCoO_2$ Cathodes, *Angew. Chem., Int. Ed.*, 2021, **60**(52), 27102–27112.
67 J. Tan, Z. Wang, G. Li, H. Hu, J. Li, R. Han and D. Zhang, Electrochemically Driven Phase Transition in $LiCoO_2$ Cathode, *Materials*, 2021, **14**(2), 242.
68 Y. Lyu, X. Wu and K. Wang, An Overview on the Advances of $LiCoO_2$ Cathodes for Lithium-Ion Batteries, *Adv. Energy Mater.*, 2021, **11**(2), 2000982.
69 N. S. Choi, Z. Chen and S. A. Freunberger, *et al.*, Challenges Facing Lithium Batteries and Electrical Double-Layer Capacitors, *Angew. Chem., Int. Ed.*, 2012, **51**(40), 9994–10024.

70 Y. Cho, J. Eom and J. Cho, High Performance $LiCoO_2$ Cathode Materials at 60 degrees C for Lithium Secondary Batteries Prepared by the Facile Nanoscale Dry-Coating Method, *J. Electrochem. Soc.*, 2013, **157**(5), A617–A624.

71 S. Deng, Y. Li, Q. Dai, J. Fu, Y. Chen, J. Zheng, T. Lei, J. Guo, J. Gao and W. Li, Structure and primary particle double-tuning by trace nano-TiO_2 for a high-performance $LiNiO_2$ cathode material, *Sustainable Energy Fuels*, 2019, **3**(11), 3234–3243.

72 J. Yin, X. Yao, G. Peng, J. Yang, Z. Huang, D. Liu, Y. Tao and X. Xu, Influence of the Li–Ge–P–S based solid electrolytes on NCA electrochemical performances in all-solid-state lithium batteries, *Solid State Ionics*, 2015, **274**, 8–11.

73 Q. Guo, J. Zheng, Y. Zhu, H. Jiang, H. Jiang, H. Wang, W. Sun, H. Sang, Y. Han and C. Zheng, Design of a fast ion-transport interlayer on cathode-electrolyte interface for solid-state lithium metal batteries, *Energy Storage Mater.*, 2022, **48**, 205–211.

74 C. Liu, G. Cao, Z. Wu, J. Hu, H. Wang and G. Shao, Surficial structure retention mechanism for $LiNi_{0.8}Co_{0.15}Al_{0.05}O_2$ in a full gradient cathode, *ACS Appl. Mater. Interfaces*, 2019, **11**(35), 31991–31996.

75 G. Girard, X. Wang, R. Yunis, P. C. Howlett and M. Forsyth, Stable performance of an all-solid-state Li metal cell coupled with a high-voltage NCA cathode and ultra-high lithium content poly(ionic liquid) s-based polymer electrolyte, *J. Solid State Electrochem.*, 2020, **24**(10), 2479–2485.

76 J. Li, J. Qi, F. Jin, F. Zhang, L. Zheng, L. Tang, R. Huang, J. Xu, H. Chen and M. Liu, Room temperature all-solid-state lithium batteries based on a soluble organic cage ionic conductor, *Nat. Commun.*, 2022, **13**(1), 1–11.

77 S. Hong, S. H. Song, M. Cho, S. Kim, S. H. Yu, D. Lee and H. Kim, Structural and Chemical Compatibilities of $Li_{1-x}Ni_{0.5}Co_{0.2}Mn_{0.3}O_2$ Cathode Material with Garnet-Type Solid Electrolyte for All-Solid-State Batteries, *Small*, 2021, **17**(46), 2103306.

78 W. Liang, Y. Shao, Y.-M. Chen and Y. Zhu, A 4 V cathode compatible, superionic conductive solid polymer electrolyte for solid lithium metal batteries with long cycle life, *ACS Appl. Energy Mater.*, 2018, **1**(11), 6064–6071.

79 W. Liu, P. Oh and X. Liu, *et al.*, Nickel-Rich Layered Lithium Transition-Metal Oxide for High-Energy Lithium-Ion Batteries, *Angew. Chem., Int. Ed.*, 2015, **54**(15), 4440–4457.

80 T. Ohzuku and Y. Makimura, Layered Lithium Insertion Material of $LiCo_{1/3}Ni_{1/3}Mn_{1/3}O_2$ for Lithium-Ion Batteries, *Chem. Lett.*, 2001, (7), 642–643.

81 P. Rozier and J. M. Tarascon, Review—Li-Rich Layered Oxide Cathodes for Next-Generation Li-Ion Batteries: Chances and Challenges, *J. Electrochem. Soc.*, 2015, **162**(14), A2490–A2499.

82 Y. Su, S. Cui and Z. Zhuo, *et al.*, Enhancing the High-Voltage Cycling Performance of $LiNi_{0.5}Mn_{0.3}Co_{0.2}O_2$ by Retarding Its Interfacial Reaction with an Electrolyte by Atomic-Layer-Deposited Al_2O_3, *ACS Appl. Mater. Interfaces*, 2015, **7**(45), 25105–25112.

83 L. A. Riley, S. V. Atta, A. S. Cavanagh, Y. Yan, S. M. George, L. Ping, A. C. Dillon and S. H. Lee, Electrochemical effects of ALD surface modification on combustion synthesized $LiNi_{1/3}Mn_{1/3}Co_{1/3}O_2$ as a layered-cathode material, *J. Power Sources*, 2011, **196**(6), 3317–3324.

84 S.-B. Kim, H. Kim, D.-H. Park, J.-H. Kim, J.-H. Shin, J.-S. Jang, S.-H. Moon, J.-H. Choi and K.-W. Park, Li-ion diffusivity and electrochemical performance of Ni-rich cathode material doped with fluoride ions, *J. Power Sources*, 2021, **506**, 230219.

85 Z. A. Wei, A. Qc, A. Yl, C. A. Chao, A. Xl, Y. A. Min, B. Rw, C. Sc and A. Sx, Enhanced electrochemical performances of $LiNi_{0.8}Co_{0.1}Mn_{0.1}O_2$ by synergistic modification of sodium ion doping and silica coating, *Solid State Ionics*, 2020, **346**, 115214.

86 G. Xu, M. Zhao, B. Xie, X. Wang, M. Jiang, P. Guan, P. Han and G. Cui, A rigid-flexible coupling gel polymer electrolyte towards high safety flexible Li-Ion battery, *J. Power Sources*, 2021, **499**, 229944.

87 J. Zheng, C. Sun, Z. Wang, S. Liu, B. An, Z. Sun and F. Li, Double Ionic–Electronic Transfer Interface Layers for All-Solid-State Lithium Batteries, *Angew. Chem., Int. Ed.*, 2021, **60**(34), 18448–18453.

88 Y. Liu, Y. Zhao, W. Lu, L. Sun, L. Lin, M. Zheng, X. Sun and H. Xie, PEO based polymer in plastic crystal electrolytes for room temperature high-voltage lithium metal batteries, *Nano Energy*, 2021, **88**, 106205.

89 J.-Y. Liang, X.-X. Zeng, X.-D. Zhang, T.-T. Zuo, M. Yan, Y.-X. Yin, J.-L. Shi, X.-W. Wu, Y.-G. Guo and L.-J. Wan, Engineering janus interfaces of ceramic electrolyte via distinct functional polymers for stable high-voltage Li-metal batteries, *J. Am. Chem. Soc.*, 2019, **141**(23), 9165–9169.

90 H. Duan, M. Fan, W. P. Chen, J. Y. Li, P. F. Wang, W. P. Wang, J. L. Shi, Y. X. Yin, L. J. Wan and Y. G. Guo, Extended electrochemical window of solid electrolytes via heterogeneous multilayered structure for high-voltage lithium metal batteries, *Adv. Mater.*, 2019, **31**(12), 1807789.

91 L. Zhou, T.-T. Zuo, C. Y. Kwok, S. Y. Kim, A. Assoud, Q. Zhang, J. Janek and L. F. Nazar, High areal capacity, long cycle life 4 V ceramic all-solid-state Li-ion batteries enabled by chloride solid electrolytes, *Nat. Energy*, 2022, **7**(1), 83–93.

92 M. Sun, Z. Zeng, W. Zhong, Z. Han, L. Peng, C. Yu, S. Cheng and J. Xie, In situ prepared ''polymer-in-salt'' electrolytes enabling high-voltage lithium metal battery, *J. Mater. Chem. A*, 2022, **10**(21), 11732–11741.

93 N. Meng, F. Lian and G. Cui, Macromolecular Design of Lithium Conductive Polymer as Electrolyte for Solid-State Lithium Batteries, *Small*, 2021, **17**(3), 2005762.

94 J. Zhang, M. Zhou, J. Shi, Y. Zhao, X. Wen, C.-C. Su, J. Wu and J. Guo, Regulating lithium deposition via electropolymerization of acrylonitrile in rechargeable lithium metal batteries, *Nano Energy*, 2021, **88**, 106298.

95 S. Liu, L. Zhou, J. Han, K. Wen, S. Guan, C. Xue, Z. Zhang, B. Xu, Y. Lin and Y. Shen, Super Long-Cycling All-Solid-State Battery with Thin Li6PS5Cl-Based Electrolyte, *Adv. Energy Mater.*, 2022, **12**(25), 2200660.

96 C. Fu, G. Homann, R. Grissa, D. Rentsch, W. Zhao, T. Gouveia, A. Falgayrat, R. Lin, S. Fantini and C. Battaglia, A Polymerized-Ionic-Liquid-Based Polymer Electrolyte with High Oxidative Stability for 4 and 5 V Class Solid-State Lithium Metal Batteries, *Adv. Energy Mater.*, 2022, **12**(27), 2200412.

97 R. Fang, B. Xu, N. S. Grundish, Y. Xia, Y. Li, C. Lu, Y. Liu, N. Wu and J. B. Goodenough, Li_2S_6-Integrated PEO-Based Polymer Electrolytes for All-Solid-State Lithium-Metal Batteries, *Angew. Chem.*, 2021, **133**(32), 17842–17847.

98 C. Niu, W. Luo, C. Dai, C. Yu and Y. Xu, High-voltage-tolerant covalent organic framework electrolyte with holistically oriented channels for solid-state lithium metal batteries with nickel-rich cathodes, *Angew. Chem., Int. Ed.*, 2021, **60**(47), 24915–24923.

99 Z. Chen, H. D. Nguyen, M. Zarrabeitia, Hp Liang, D. Geiger, J. K. Kim, U. Kaiser, S. Passerini, C. Iojoiu and D. Bresser, Lithium Phosphonate Functionalized Polymer Coating for High-Energy $Li[Ni_{0.8}Co_{0.1}Mn_{0.1}]O_2$ with Superior Performance at Ambient and Elevated Temperatures, *Adv. Funct. Mater.*, 2021, **31**(41), 2105343.

100 F. Cheng, X. Zhang, Y. Qiu, J. Zhang, Y. Liu, P. Wei, M. Ou, S. Sun, Y. Xu and Q. Li, Tailoring electrolyte to enable high-rate and super-stable Ni-rich NCM cathode materials for Li-ion batteries, *Nano Energy*, 2021, **88**, 106301.

101 H. Y. Su, K. S. Park and J. P. Yong, The electrochemical property of ZrF_x-coated $Li[Ni_{1/3}Co_{1/3}Mn_{1/3}]O_2$ cathode material, *J. Power Sources*, 2010, **195**(18), 6108–6115.

102 X. Yang, X. Wang, L. Hu, G. Zou, S. Su, Y. Bai, H. Shu, Q. Wei, B. Hu and L. Ge, Layered $Li[Ni_{0.5}Co_{0.2}Mn_{0.3}]O_2$–$Li_2MnO_3$ core–shell structured cathode material with excellent stability, *J. Power Sources*, 2013, **242**(NOV. 15), 589–596.

103 H.-H. Ryu, K.-J. Park, C. S. Yoon and Y.-K. Sun, Capacity Fading of Ni-Rich $Li[Ni_xCo_yMn_{1-x-y}]O_2$ ($0.6 \leq x \leq 0.95$) Cathodes for High-Energy-Density Lithium-Ion Batteries: Bulk or Surface Degradation?, *Chem. Mater.*, 2018, **30**(3), 1155–1163.

104 X. Wang, Y. L. Ding, Y. P. Deng and Z. Chen, Ni-Rich/Co-Poor Layered Cathode for Automotive Li-Ion Batteries: Promises and Challenges, *Adv. Energy Mater.*, 2020, **10**(12), 1903864.

105 J. Kim, H. Lee, H. Cha, M. Yoon, M. Park and J. Cho, Prospect and Reality of Ni-Rich Cathode for Commercialization, *Adv. Energy Mater.*, 2018, **8**(6), 1702028.

106 T. Hatsukade, A. Schiele, P. Hartmann, T. Brezesinski and J. Janek, The Origin of Carbon Dioxide Evolved during Cycling of Nickel-Rich Layered NCM Cathodes, *ACS Appl. Mater. Interfaces*, 2018, **10**(45), 38892–38899.

107 M. Yi, J. Li, X. Fan, M. Bai, Z. Zhang, B. Hong, Z. Zhang, G. Hu, H. Jiang and Y. Lai, Single crystal Ni-rich layered cathodes enabling superior performance in all-solid-state batteries with PEO-based solid electrolytes, *J. Mater. Chem. A*, 2021, **9**(31), 16787–16797.

108 X. Li, L. Jin, D. Song, H. Zhang, X. Shi, Z. Wang, L. Zhang and L. Zhu, $LiNbO_3$-coated $LiNi_{0.8}Co_{0.1}Mn_{0.1}O_2$ cathode with high discharge capacity and rate performance for all-solid-state lithium battery, *J. Energy Chem.*, 2020, **40**, 39–45.

109 K. Heo, J. Lee, J. Im, M.-Y. Kim, H.-S. Kim, D. Ahn, J. Kim and J. Lim, A composite cathode material encapsulated by amorphous garnet-type solid electrolyte and self-assembled $La_2(Ni_{0.5}Li_{0.5})O_4$ nanoparticles for all-solid-state batteries, *J. Mater. Chem. A*, 2020, **8**(43), 22893–22906.

110 A. Manthiram, K. Chemelewski and E. S. Lee, A perspective on the high-voltage $LiMn_{1.5}Ni_{0.5}O_4$ spinel cathode for lithium-ion batteries, *Energy Environ. Sci.*, 2013, **7**(4), 1339–1350.

111 A. Perea, K. Zaghib and D. Belanger, Characterization of $LiNi_{0.5}Mn_{1.5}O_4$ spinel electrode in the presence of 1,3,5-trihydroxybenzene as additive, *J. Mater. Chem. A*, 2015, **3**(6), 2776–2783.

112 L. Yang, B. Ravdel and B. L. Lucht, Electrolyte Reactions with the Surface of High Voltage $LiNi_{0.5}Mn_{1.5}O_4$ Cathodes for Lithium-Ion Batteries, *Electrochem. Solid-State Lett.*, 2010, **13**(8), A95–A97.

113 R. Zhu, S. Zhang, Q. Guo, Y. Zhou, J. Li, P. Wang and Z. Gong, More than just a protection layer: inducing chemical interaction between Li_3BO_3 and $LiNi_{0.5}Mn_{1.5}O_4$ to achieve stable high-rate cycling cathode materials, *Electrochim. Acta*, 2020, **342**, 136074.

114 S. Wang, J. Guo, Y. Li, D. Zhang, C. Li, X. Ren, S. Liu, Y. Xiong, S. Hao and J. Zheng, Achieving superior high-rate cyclability of $LiNi_{0.5}Mn_{1.5}O_4$ cathode material via constructing stable CuO modification interface, *J. Electroanal. Chem.*, 2020, **903**, 115825.

115 F. Li, J. Ma, J. Lin, X. H. Zhang and G. Yang, Exploring the origin of electrochemical performance of Cr-doped $LiNi_{0.5}Mn_{1.5}O_4$, *Phys. Chem. Chem. Phys.*, 2020, **22**(7), 3831–3838.

116 R. Shimizu, D. Cheng, J. L. Weaver, M. Zhang, B. Lu, T. A. Wynn, R. Burger, Mc Kim, G. Zhu and Y. S. Meng, Unraveling the Stable Cathode Electrolyte Interface in all Solid-State Thin-Film Battery Operating at 5 V, *Adv. Energy Mater.*, 2022, **12**(31), 2201119.

117 J. H. Kim, J. W. Jung, S. H. Cho, I. D. Kim, Y. C. Park, D. H. Seo and H. S. Kim, Investigation of Ordering on Oxygen-Deficient LiNi(0.5) Mn(1.5) O(4-delta) Thin Films for Boosting Electrochemical Performance in All-Solid-State Thin-Film Batteries, *Small*, 2022, **18**(24), 2201134.

118 L. Xiong, G. Chen, Y. Tang, J. Hao and W. Cui, Equation of state of $LiNi_{0.5}Mn_{1.5}O_4$ at high pressure, *Solid State Commun.*, 2020, **321**, 114045.

119 Y. Zuo, B. Li, N. Jiang, W. Chu, H. Zhang, R. Zou and D. Xia, A High-Capacity O_2-Type Li-Rich Cathode Material with a Single-Layer Li_2MnO_3 Superstructure, *Adv. Mater.*, 2018, **30**(16), 1707255.

120 X. Yu, Y. Lyu, L. Gu, H. Wu, S. M. Bak, Y. Zhou, K. Amine, S. N. Ehrlich, H. Li and K. W. Nam, Understanding the rate capability of high-energy-density Li-rich layered $Li_{1.2}Ni_{0.15}Co_{0.1}Mn_{0.55}O_2$ cathode materials, *Adv. Energy Mater.*, 2014, **4**(5), 1300950.

121 K. S. Park, A. Benayad, M. S. Park, W. Choi and D. Im, Suppression of O_2 evolution from oxide cathode for lithium-ion batteries: VO(x)-impregnated $0.5Li_2MnO_3$-$0.5LiNi_{(0.4)}Co_{(0.2)}Mn_{(0.4)}O_2$ cathode, *Chem. Commun.*, 2010, **46**(23), 4190.

122 A. Zhu, Q. Wang, Y. Zhang, Y. Zhang, X. He, K. Wu, H. Wu, Q. Wang, W. Cai and Y. Zhang, In situ formation of $Li_{0.5}Mn_{0.5}O$ coating layer through defect controlling for high performance Li-rich manganese-based cathode material, *J. Energy Chem.*, 2022, **71**, 384–391.

123 K. Luo, M. R. Roberts, R. Hao, N. Guerrini, D. M. Pickup, Y. S. Liu, K. Edstrom, J. Guo, A. V. Chadwick and L. C. Duda, Charge-compensation in 3d-transition-metal-oxide intercalation cathodes through the generation of localized electron holes on oxygen, *Nat. Chem.*, 2016, **8**(7), 684–691.

124 M. Sathiya, G. Rousse, K. Ramesha, C. P. Laisa, H. Vezin, M. T. Sougrati, M. L. Doublet, D. Foix, D. Gonbeau and W. Walker, Reversible anionic redox chemistry in high-capacity layered-oxide electrodes, *Nat. Mater.*, 2013, **12**(9), 827–835.

125 H. Jihyun, L. Hee-Dae and L. Minah, Critical Role of Oxygen Evolved from Layered Li-Excess Metal Oxides in Lithium Rechargeable Batteries, *Chem. Mater. A Pub. Am. Chem. Soc.*, 2012, **24**(14), 2692–2697.

126 N. Yabuuchi, K. Yoshii, S. T. Myung, I. Nakai and S. Komaba, Detailed studies of a high-capacity electrode material for rechargeable batteries, Li_2MnO_3-$LiCo_{(1/3)}Ni_{(1/3)}Mn_{(1/3)}O_2$, *J. Am. Chem. Soc.*, 2011, **133**(12), 4404.

127 H. Yu and H. Zhou, High-Energy Cathode Materials (Li_2MnO_3-$LiMO_2$) for Lithium-Ion Batteries, *J. Phys. Chem. Lett.*, 2013, **4**(8), 1268–1280.

128 S. Chen, Z. Gao and T. Sun, Safety challenges and safety measures of Li-ion batteries, *Energy Sci. Eng.*, 2021, **9**(9), 1647–1672.

129 Z. P. Cano, D. Banham, S. Ye, A. Hintennach, J. Lu, M. Fowler and Z. Chen, Batteries and fuel cells for emerging electric vehicle markets, *Nat. Energy*, 2018, **3**(4), 279–280.

130 M. Forsyth, L. Porcarelli, X. Wang, N. Goujon and D. Mecerreyes, Innovative Electrolytes Based on Ionic Liquids and Polymers for Next-Generation Solid-State Batteries, *Acc. Chem. Res.*, 2019, **52**(3), 686–694.

131 A. Manthiram, X. Yu and S. Wang, Lithium battery chemistries enabled by solid-state electrolytes, *Nat. Rev. Mater.*, 2017, **2**(4), 1–16.

132 B. Singh, S. Ghosh, S. Aich and B. Roy, Low temperature solid oxide electrolytes (LT-SOE): a review, *J. Power Sources*, 2017, **339**, 103–135.

133 A. Arabac, Conductivity properties of lanthanide-co-doped ceria-based solid oxide electrolytes, *Ionics*, 2019, **25**(10), 4841–4850.

134 S. Xu, Z. Sun and C. Sun, *et al.* Homogeneous and Fast Ion Conduction of PEO-Based Solid-State Electrolyte at Low Temperature, *Adv. Funct. Mater.*, 2020, **30**(51), 2007172.

135 Y. Meng, C. Qrab, C. Tya, D. Hzabc and C. Szab, Solid polymer electrolyte with in situ generated fast Li^+ conducting network enable high voltage and dendrite-free lithium metal battery, *Energy Storage Mater.*, 2022, **44**, 93–103.

136 L. Zhu, P. Zhu, L. You and S. Li, Bamboo shoot skin: turning waste to a valuable adsorbent for the removal of cationic dye from aqueous solution, *Clean Technol. Environ. Policy*, 2019, **21**(1), 81–92.

137 L. Zhu, P. Zhu, Q. Fang, M. Jing, X. Shen and L. Yang, A novel solid PEO/LLTO-nanowires polymer composite electrolyte for solid-state lithium-ion battery, *Electrochim. Acta*, 2018, **292**, 718–726.

138 L. Zhu, P. Zhu, S. Yao, X. Shen and F. Tu, High-performance solid PEO/PPC/LLTO-nanowires polymer composite electrolyte for solid-state lithium battery, *Int. J. Energy Res.*, 2019, **43**(9), 4854–4866.

139 L. Li, H. Duan, J. Li, L. Zhang and G. Chen, Toward High Performance All solid state Lithium Batteries with High voltage Cathode Materials: Design Strategies for Solid Electrolytes, Cathode Interfaces, and Composite Electrodes, *Adv. Energy Mater.*, 2021, **11**(28), 2003154.

140 Y. Lin, Y. Cheng, J. Li, J. D. Miller, J. Liu and X. Wang, Biocompatible and biodegradable solid polymer electrolytes for high voltage and high temperature lithium batteries, *RSC Adv.*, 2017, **7**(40), 24856–24863.

141 W. Zhou, Z. Wang, Y. Pu, Y. Li and J. B. Goodenough, Double-Layer Polymer Electrolyte for High-Voltage All-Solid-State Rechargeable Batteries, *Adv. Mater.*, 2019, **31**(4), 1805574.

142 H. Duan, M. Fan, W. Chen, J. Li, P. Wang, W. Wang, J. Shi, Y. Yin, L. Wan and Y. Guo, Extended Electrochemical Window of Solid Electrolytes via Heterogeneous Multilayered Structure for High-Voltage Lithium Metal Batteries, *Adv. Mater.*, 2019, **31**(12), 1807789.

143 C. Wang, T. Wang, L. Wang, Z. Hu, Z. Cui, J. Li, S. Dong, X. Zhou and G. Cui, Differentiated lithium salt design for multilayered PEO electrolyte enables a high-voltage solid-state lithium metal battery, Advanced, *Science*, 2019, **6**(22), 1901036.

144 D. Qwa, A. Zc, Z. A. Qian, D. Xsa, A. Xd, A. Sd, B. Lq, C. Sh, A. Xl and B. Kt, A supramolecular interaction strategy enabling high-performance all solid state electrolyte of lithium metal batteries, *Energy Storage Mater.*, 2020, **25**, 756–763.

145 A. Bz, A. Yz, Z. A. Ning, A. Jl, A. Lc, L. A. Jia, A. Ls, B. Am, B. Cmj and A. Hx, Synthesis and interface stability of polystyrene-poly(ethylene glycol)-polystyrene triblock copolymer as solid-state electrolyte for lithium-metal batteries, *J. Power Sources*, 2019, **428**, 93–104.

146 H. Chen, D. Adekoya, L. Hencz, J. Ma and S. Zhang, Stable Seamless Interfaces and Rapid Ionic Conductivity of Ca–CeO_2/LiTFSI/PEO Composite Electrolyte for High voltate and High voltage All solid state Battery, *Laser Phys. Rev.*, 2020, **10**(21), 2000049.

147 J. Sun and C. He, Hierarchical Composite-Solid-Electrolyte with High Electrochemical Stability and Interfacial Regulation for Boosting Ultra-Stable Lithium Batteries, *Adv. Funct. Mater.*, 2021, **31**(1), 2006381.

148 Y. Wang, L. Wu, Z. Lin, M. Tang, P. Ding, X. Guo, Z. Zhang, S. Liu, B. Wang and X. Yin, Hydrogen bonds enhanced composite polymer electrolyte for high-voltage cathode of solid-state lithium battery, *Nano Energy*, 2022, **96**, 107105.
149 H. A. Hoang and D. Kim, High voltage stable solid-state lithium battery based on the nano-conductor imbedded flexible hybrid solid electrolyte with hyper-ion conductivity and thermal, mechanical, and adhesive stability, *Chem. Eng. J.*, 2022, **435**, 135092.
150 H. Li, Y. Du, X. Wu, J. Xie and F. Lian, Developing ''Polymer-in-Salt'' High Voltage Electrolyte Based on Composite Lithium Salts for Solid-State Li Metal Batteries, *Adv. Funct. Mater.*, 2021, **31**(41), 2103409.
151 J. Pan, Y. Zhang, J. Wang, Z. Bai, R. Cao, N. Wang, S. Dou and F. Huang, A Quasi-Double-Layer Solid Electrolyte with Adjustable Interphases Enabling High-Voltage Solid-State Batteries, *Adv. Mater.*, 2022, **34**(10), 2107183.
152 C. Wang, R. Yu, H. Duan, Q. Lu, Q. Li, K. R. Adair, D. Bao, Y. Liu, R. Yang and J. Wang, Solvent-Free Approach for Interweaving Freestanding and Ultrathin Inorganic Solid Electrolyte Membranes, *ACS Energy Lett.*, 2021, **7**, 410–416.
153 S. Y. Kim, K. Kaup, K.-H. Park, A. Assoud, L. Zhou, J. Liu, X. Wu and L. F. Nazar, Lithium ytterbium-based halide solid electrolytes for high voltage all-solid-state batteries, ACS, *Mater. Lett.*, 2021, **3**(7), 930–938.
154 Q. Zhang, X. Liu, H. Li, Z. Guo, T. Bian, X. Zhu, N. Zhan and Y. Zhao, A Multifunctional Silicon-Doped Polyether Network for Double Stable Interfaces in Quasi-Solid-State Lithium Metal Batteries, *Small*, 2022, **18**(11), 2106395.
155 Z. Li, S. Weng, J. Fu, X. Wang, X. Zhou, Q. Zhang, X. Wang, L. Wei and X. Guo, Nonflammable quasi-solid electrolyte for energy-dense and long-cycling lithium metal batteries with high-voltage Ni-rich layered cathodes, *Energy Storage Mater.*, 2022, **47**, 542–550.
156 H. P. Liang, M. Zarrabeitia, Z. Chen, S. Jovanovic, S. Merz, J. Granwehr, S. Passerini and D. Bresser, Polysiloxane-Based Single-Ion Conducting Polymer Blend Electrolyte Comprising Small-Molecule Organic Carbonates for High-Energy and High-Power Lithium-Metal Batteries, *Adv. Energy Mater.*, 2022, **12**(16), 2200013.
157 H. Wang, T. Hou, H. Cheng, B. Jiang, H. Xu and Y. Huang, Bifunctional LiI additive for poly(ethylene oxide) electrolyte with high ionic conductivity and stable interfacial chemistry, *J. Energy Chem.*, 2022, **71**, 218–224.
158 Z. Lin, X. Guo, R. Zhang, M. Tang, P. Ding, Z. Zhang, L. Wu, Y. Wang, S. Zhao and Q. Zhang, Molecular structure adjustment enhanced anti-oxidation ability of polymer electrolyte for solid-state lithium metal battery, *Nano Energy*, 2022, **98**, 107330.
159 L. Li, H. Duan, J. Li, L. Zhang, Y. Deng and G. Chen, Toward High Performance All-Solid-State Lithium Batteries with High-Voltage Cathode Materials: Design Strategies for Solid Electrolytes, Cathode Interfaces, and Composite Electrodes, *Adv. Energy Mater.*, 2021, **11**(28), 2003154.
160 X. He, Y. Mo and Y. Zhu, First principles study on electrochemical and chemical stability of solid electrolyte-electrode interfaces in all-solid-state Li-ion batteries, *J. Mater. Chem. A*, 2016, **4**(9), 3253–3266.
161 J. Duan, L. Huang, T. Wang, Y. Huang, H. Fu, W. Wu, W. Luo and Y. Huang, Shaping the contact between Li metal anode and solid-state electrolytes, *Adv. Funct. Mater.*, 2020, **30**(15), 1908701.
162 F. Han, Y. Zhu, X. He, Y. Mo and C. Wang, Electrochemical Stability of $Li_{10}GeP_2S_{12}$ and $Li_7La_3Zr_2O_{12}$ Solid Electrolytes, *Adv. Energy Mater.*, 2016, **6**(8), 1501590.
163 Y. Li, W. Zheng, C. Yang, F. Du and X. Guo, W-Doped Li7La3Zr2O12 Ceramic Electrolytes for Solid State Li-ion Batteries, *Electrochim. Acta*, 2015, **180**, 37–42.
164 V. Thangadurai, D. Pinzaru, S. Narayanan and A. K. Baral, Fast Solid-State Li Ion Conducting Garnet-Type Structure Metal Oxides for Energy Storage, *J. Phys. Chem. Lett.*, 2015, **6**(2), 292.
165 C. Hnsel, S. Afyon and J. Rupp, Investigating the all-solid-state batteries based on lithium garnets and a high potential cathode – $LiMn_{1.5}Ni_{0.5}O_4$, *Nanoscale*, 2016, **8**(43), 18412–18420.
166 Z. Liu, W. Fu, E. A. Payzant, Y. Xiang, Z. Wu, N. J. Dudney, J. Kiggans, K. Hong, A. J. Rondinone and C. Liang, Anomalous high ionic conductivity of nanoporous β-Li_3PS_4, *J. Am. Chem. Soc.*, 2013, **135**(3), 975–978.
167 Y. Seino, T. Ota, K. Takada, A. Hayashi and M. Tatsumisago, A sulphide lithium super ion conductor is superior to liquid ion conductors for use in rechargeable batteries, *Energy Environ. Sci.*, 2014, **7**(2), 627–631.
168 R. Koerver, I. Aygün, T. Leichtweiß, C. Dietrich, W. Zhang, J. O. Binder, P. Hartmann, W. G. Zeie and J. Janek, Capacity Fade in Solid-State Batteries: Interphase Formation and Chemomechanical Processes in Nickel-Rich Layered Oxide Cathodes and Lithium Thiophosphate Solid Electrolytes, *Chem. Mater.*, 2017, **29**(13), 5574–5582.
169 A. Banerjee, H. Tang, X. Wang, J. H. Cheng and Y. S. Meng, Revealing Nanoscale solid–solid Interfacial Phenomena for Long-Life and High-Energy All-Solid-State Batteries, *ACS Appl. Mater. Interfaces*, 2019, **11**(46), 43138–43145.
170 T. Swamy, X. Chen and Y.-M. Chiang, Electrochemical Redox Behavior of Li Ion Conducting Sulfide Solid Electrolytes, *Chem. Mater.*, 2019, **31**(3), 707–713.
171 G. F. Dewald, S. Ohno and M. A. Kraft, *et al.*, Experimental Assessment of the Practical Oxidative Stability of Lithium Thiophosphate Solid Electrolytes, *Chem. Mater.*, 2019, **31**(20), 8328–8337.
172 Y. Wang, Y. Lv, Y. Su, L. Chen, H. Li and F. Wu, 5 V-class sulfurized spinel cathode stable in sulfide all-solid-state batteries, *Nano Energy*, 2021, **90**, 106589.
173 L. Zhou, T.-T. Zuo, C. Y. Kwok, S. Y. Kim, A. Assoud, Q. Zhang, J. Janek and L. F. Nazar, High areal capacity, long cycle life 4 V ceramic all-solid-state Li-ion batteries enabled by chloride solid electrolytes, *Nat. Energy*, 2022, **7**(1), 83–93.
174 S. Y. Kim, K. Kaup, K. H. Park, A. Assoud and L. F. Nazar, Lithium Ytterbium-Based Halide Solid Electrolytes for High Voltage All-Solid-State Batteries, ACS, *Mater. Lett.*, 2021, **3**(7), 930–938.

175 X. Zheng, E.-D. Fu, P. Chen, S. Liu, G.-R. Li and X.-P. Gao, Li_3InCl_6-coated $LiCoO_2$ for high-performance all solid-state batteries, *Appl. Phys. Lett.*, 2022, **121**(3), 033902.

176 I. Kochetkov, T.-T. Zuo, R. Ruess, B. Singh, L. Zhou, K. Kaup, J. Janek and L. Nazar, Different interfacial reactivity of lithium metal chloride electrolytes with high voltage cathodes determines solid-state battery performance, *Energy Environ. Sci.*, 2022, **15**(9), 3933–3944.

177 C. Sun, J. Liu, Y. Gong, D. P. Wilkinson and J. Zhang, Recent advances in all-solid-state rechargeable lithium batteries, *Nano Energy*, 2017, **33**, 363–386.

178 K. S. Ngai, S. Ramesh, K. Ramesh and J. C. Juan, A review of polymer electrolytes: fundamental, approaches and applications, *Ionics*, 2016, **22**, 1259–1279.

179 Selectively Wetted Rigid–Flexible Coupling Polymer Electrolyte Enabling Superior Stability and Compatibility of High-Voltage Lithium Metal Batteries, *Adv. Energy Mater.*, 2020, **10**(18), 1903939.

180 W. Liang, Y. Shao, Y. M. Chen and Y. Zhu, A 4 V Cathode Compatible, Superionic Conductive Solid Polymer Electrolyte for Solid Lithium Metal Batteries with Long Cycle Life, *ACS Appl. Energy Mater.*, 2018, **1**(11), 6064–6071.

181 J. Zhang, X. Zang, H. Wen, T. Dong, J. Chai, Y. Li, B. Chen, J. Zhao, S. Dong, J. Ma, L. Yue, Z. Liu, X. Guo, G. Cui and L. Chen, High-voltage and free-standing poly(propylene carbonate)/$Li_{6.75}La_3Zr_{1.75}Ta_{0.25}O_{12}$ composite solid electrolyte for wide temperature range and flexible solid lithium ion battery, *J. Mater. Chem. A*, 2017, **5**(10), 4940–4948.

182 W. Liu, C. Yi and L. Li, Designing Polymer-in-Salt Electrolyte and Fully Infiltrated 3D Electrode for Integrated Solid-State Lithium Batteries, *Angew. Chem., Int. Ed.*, 2021, **133**(23), 13041–13050.

183 H. Zhai, B. Qie, Q. Cheng, A. Li, J. Borovilas, B. Xu, C. Shi, T. Jin and X. Liao, Rechargeable solid-state lithium metal batteries with vertically aligned ceramic nanoparticle/polymer composite electrolyte, *Nano Energy*, 2019, **60**, 205–212.

184 S. Li, S. Q. Zhang, L. Shen, Q. Liu, J. B. Ma, W. Lv, Y. B. He and Q. H. Yang, Progress and Perspective of Ceramic/Polymer Composite Solid Electrolytes for Lithium Batteries, *Adv. Sci.*, 2020, **7**(5), 1903088.

185 M. Dirican, C. Yan, P. Zhu and X. Zhang, Composite solid electrolytes for all-solid-state lithium batteries, *Mater. Sci. Eng., R*, 2019, **136**, 27–46.

186 M. B. Dixit, W. Zaman, N. Hortance, S. Vujic, B. Harkey, F. Shen, W. Y. Tsai, V. D. Andrade, X. C. Chen and N. Balke, Nanoscale Mapping of Extrinsic Interfaces in Hybrid Solid Electrolytes, *Joule*, 2020, **4**(1), 207–221.

187 A. Li, X. Liao, H. Zhang, L. Shi, P. Wang, Q. Cheng, J. Borovilas, Z. Li, W. Huang and Z. Fu, Nacre-Inspired Composite Electrolytes for Load-Bearing Solid-State Lithium-Metal Batteries, *Adv. Mater.*, 2020, **32**(2), 1905517.

188 M. Falco, L. Castro, J. R. Nair, F. Bella, F. Barde, G. Meligrana and C. Gerbaldi, UV-Cross-Linked Composite Polymer Electrolyte for High-Rate, Ambient Temperature Lithium Batteries, *ACS Appl. Energy Mater.*, 2019, **2**(3), 1600–1607.

189 K. Liu, M. Wu, H. Jiang, Y. Lin and T. Zhao, An ultrathin, strong, flexible composite solid electrolyte for high-voltage lithium metal batteries, *J. Mater. Chem. A*, 2020, **8**(36), 18802–18809.

190 Y. Li, W. Zhang, Q. Dou, K. W. Wong and K. M. Ng, $Li_7La_3Zr_2O_{12}$ ceramic nanofiber-incorporated composite polymer electrolytes for lithium metal batteries, *J. Mater. Chem. A*, 2019, **7**(7), 3391–3398.

191 B. Sza, L. B. Zheng, G. Yue, B. Lc, B. Pm, C. Kz, L. A. Ying and B. Vgp, Room-temperature, high-voltage solid-state lithium battery with composite solid polymer electrolyte with in situ thermal safety study - ScienceDirect, *Chem. Eng. J.*, 2020, **400**, 125996.

192 C. Z. Zhao, X. Q. Zhang, X. B. Cheng, R. Zhang, R. Xu, P. Y. Chen, H. J. Peng, J. Q. Huang and Q. Zhang, An anion-immobilized composite electrolyte for dendrite-free lithium metal anodes, *Proc. Natl. Acad. Sci. U. S. A.*, 2017, **114**(42), 11069–11074.

193 C. Li, S. Zhou, L. Dai, X. Zhou, B. Zhang, L. Chen, T. Zeng, Y. Liu, Y. Tang, J. Jiang and J. Huang, Porous polyamine/PEO composite solid electrolyte for high performance solid-state lithium metal batteries, *J. Mater. Chem. A*, 2021, **9**(43), 24661–24669.

194 C. Li, Y. Huang, X. Liu, C. Chen, X. Feng, Z. Zhang and P. Liu, Composite solid electrolyte with Li^+ conducting 3D porous garnet-type framework for all-solid-state lithium batteries, *Mater. Chem. Front.*, 2022, **6**(12), 1672–1680.

195 R. Lei, Y. Yang, C. Yu, Y. Xu, Y. Li and J. Li, A facile preparation of PEO–$LiClO_4$–fumed SiO_2 composite solid-state electrolyte with improved electrochemical performance for lithium-metal batteries, Sustainable, *Energy Fuels*, 2021, **5**(5), 1538–1547.

196 H. Fan, F. Wei, J. Luo, S. Wu, X. Jian, W. Lan, K. Zhang, R. Zeng, H. Chen and R. Zhao, Interfacial engineering facilitating robust $Li_{6.35}Ga_{0.15}La_3Zr_{1.8}Nb_{0.2}O_{12}$ for all-solid-state lithium batteries, *Sustainable Energy Fuels*, 2021, **5**(7), 2077–2084.

197 Z. Deng, D. Ni, D. Chen, Y. Bian, S. Li, Z. Wang and Y. Zhao, Anti-perovskite materials for energy storage batteries, *InfoMat*, 2021, **4**(2), e12252.

198 G. L. Zhu, C. Z. Zhao, H. J. Peng, H. Yuan, J. K. Hu, H. X. Nan, Y. Lu, X. Y. Liu, J. Q. Huang, C. He, J. Zhang and Q. Zhang, A Self-Limited Free-Standing Sulfide Electrolyte Thin Film for All-Solid-State Lithium Metal Batteries, *Adv. Funct. Mater.*, 2021, **31**(32), 2101985.

199 K. Yang, L. Chen, J. Ma, Y. B. He and F. Kang, Progress and perspective of $Li_{1+x}Al_xTi_{2-x}(PO_4)_3$ ceramic electrolyte in lithium batteries, *InfoMat*, 2021, **3**(11), 1195–1217.

200 D. Atkins, E. Ayerbe, A. Benayad, F. G. Capone, E. Capria, I. E. Castelli, I. Cekic-Laskovic, R. Ciria, L. Dudy, K. Edström, M. R. Johnson, H. Li, J. M. G. Lastra, M. L. De Souza, V. Meunier, M. Morcrette, H. Reichert, P. Simon, J. P. Rueff, J. Sottmann, W. Wenzel and A. Grimaud, Understanding Battery Interfaces by Combined Characterization and Simulation Approaches: Challenges and Perspectives, *Adv. Energy Mater.*, 2022, **12**(17), 2102687.

201 K. Song and W. Chen, An effective solid–electrolyte interphase for stable solid-state batteries, *Chem*, 2021, **7**(12), 3195–3197.
202 L. Peng, C. Yu and Z. Zhang, Tuning solid interfaces via varying electrolyte distributions enables high performance solid-state batteries, *Energy Environ. Mater.*, 2022, **0**, 1–8.
203 D. Tan, A. Banerjee, Z. Chen and Y. S. Meng, From nanoscale interface characterization to sustainable energy storage using all-solid-state batteries, *Nat. Nanotechnol.*, 2020, **15**(3), 170–180.
204 C. Wang, R. Yu, H. Duan, Q. Lu, Q. Li, K. R. Adair, D. Bao, Y. Liu, R. Yang and J. Wang, Solvent-Free Approach for Interweaving Freestanding and Ultrathin Inorganic Solid Electrolyte Membranes, *ACS Energy Lett.*, 2021, **7**(1), 410–416.
205 B. Zaid, D. Saidi, A. Benzaid and S. Hadji, Effects of pH and chloride concentration on pitting corrosion of AA6061 aluminum alloy, *Corros. Sci.*, 2008, **50**(7), 1841–1847.
206 A. Younis, M. El-Sabbah and R. Holze, The effect of chloride concentration and pH on pitting corrosion of AA7075 aluminum alloy coated with phenyltrimethoxysilane, *J. Solid State Electrochem.*, 2012, **16**(3), 1033–1040.
207 A. S. El-Amoush, Intergranular corrosion behavior of the 7075-T6 aluminum alloy under different annealing conditions, *Mater. Chem. Phys.*, 2011, **126**(3), 607–613.
208 Y. Luo, X. J. Xu, Y. K. Zhang, T. Song, H. Y. Wang, Z. Q. Zhang, F. B. Zhang, G. C. Wu and Y. Wu, Effect of Enhanced-Solid-Solution on Intergranular Corrosion and Exfoliation Corrosion Properties of 7085 Type Aluminum Alloy Containing Strontium, *J. Aeronautical Mater.*, 2012, **32**(5), 262–265.
209 D. Wang and Z. Y. Ma, Effect of pre-strain on microstructure and stress corrosion cracking of over-aged 7050 aluminum alloy, *J. Alloys Compds.*, 2009, **469**(1–2), 445–450.
210 E. C. Cormack, The Effect of Sensitization on the Stress Corrosion Cracking of Aluminum Alloy 5456, thesis collection, 2012.
211 A. Y. Musa, A. B. Mohamad, A. A. Al-Amiery and L. T. Tien, Galvanic corrosion of aluminum alloy (Al_2O_{24}) and copper in 1.0 M hydrochloric acid solution, *Korean J. Chem. Eng.*, 2012, **29**(6), 818–822.
212 Y. Yang, Y. Gu, L. Zhang, X. Jiao and J. Che, Influence of MAO Treatment on the Galvanic Corrosion Between Aluminum Alloy and 316L Steel, *J. Mater. Eng. Perf.*, 2017, **26**, 6099–6106.
213 J. Qiu, X. Liu and R. Chen, *et al.*, Enabling Stable Cycling of 4.2 V High-Voltage All-Solid-State Batteries with PEO-Based Solid Electrolyte, *Adv. Funct. Mater.*, 2020, **30**(22), 1909392.
214 K. Park, B. C. Yu and J. W. Jung, *et al.*, Electrochemical Nature of the Cathode Interface for a Solid-State Lithium-Ion Battery: interface between $LiCoO_2$ and Garnet-$Li_7La_3Zr_2O_{12}$, *Chem. Mater.*, 2016, **28**(21), 8051–8059.
215 J. Liang, Z. Yipeng, Q. Yang, Z. Jing and X. Feipeng, Engineering the conductive carbon/PEO interface to stabilize solid polymer electrolytes for all-solid-state high voltage $LiCoO_2$ batteries, *J. Mater. Chem. A*, 2020, **8**(5), 2769–2776.
216 S. Seki, Y. Kobayashi, H. Miyashiro, Y. Mita and T. Iwahori, Fabrication of High-Voltage, High-Capacity All-Solid-State Lithium Polymer Secondary Batteries by Application of the Polymer Electrolyte/Inorganic Electrolyte Composite Concept, *Chem. Mater.*, 2005, **17**(8), 2041–2045.
217 H. Miyashiro, Y. Kobayashi, S. Seki, Y. Mita, A. Usami, M. Nakayama and M. Wakihara, Fabrication of All-Solid-State Lithium Polymer Secondary Batteries Using Al_2O_3-Coated $LiCoO_2$, *Chem. Mater.*, 2010, **17**(23), 5603–5605.
218 J. Ma, Z. Liu, B. Chen, L. Wang, L. Yue, H. Liu, J. Zhang, Z. Liu and G. Cui, A strategy to make high voltage $LiCoO_2$ compatible with polyethylene oxide electrolyte in all-solid-state lithium ion batteries, *J. Electrochem. Soc.*, 2017, **164**(14), A3454.
219 Q. Yang, J. Huang, Y. Li, Y. Wang, J. Qiu, J. Zhang, H. Yu, X. Yu, H. Li and L. Chen, Surface-protected $LiCoO_2$ with ultrathin solid oxide electrolyte film for high-voltage lithium ion batteries and lithium polymer batteries, *J. Power Sources*, 2018, **388**, 65–70.
220 X. Wang, Y. Song, X. Jiang, Q. Liu, J. Dong, J. Wang, X. Zhou, B. Li, G. Yin and Z. Jiang, Constructing Interfacial Nanolayer Stabilizes 4.3 V High-Voltage All-Solid-State Lithium Batteries with PEO-Based Solid-State Electrolyte, *Adv. Funct. Mater.*, 2022, **32**(23), 2113068.
221 Q. Liu, B. Cai, S. Li, Q. Yu, F. Lv, F. Kang, Q. Wang and B. Li, Long-cycling and safe lithium metal batteries enabled by the synergetic strategy of ex situ anodic pretreatment and an in-built gel polymer electrolyte, *J. Mater. Chem. A*, 2020, **8**(15), 7197–7204.
222 X. Lin, J. Yu, M. B. Effat, G. Zhou, M. J. Robson, S. C. Kwok, H. Li, S. Zhan, Y. Shang and F. Ciucci, Ultrathin and Non-Flammable Dual-Salt Polymer Electrolyte for High-Energy-Density Lithium-Metal Battery, *Adv. Funct. Mater.*, 2021, **31**(17), 2010261.
223 L. P. Wang, X. D. Zhang and T. S. Wang, *et al.*, Ameliorating the Interfacial Problems of Cathode and Solid-State Electrolytes by Interface Modification of Functional Polymers, *Adv. Energy Mater.*, 2018, **8**(24), 1801528.
224 J. Lu, J. Zhou, R. Chen, F. Fang, K. Nie, W. Qi, J.-N. Zhang, R. Yang, X. Yu and H. Li, 4.2 V poly (ethylene oxide)-based all-solid-state lithium batteries with superior cycle and safety performance, *Energy Storage Mater.*, 2020, **32**, 191–198.
225 J. Qiu, L. Yang, G. Sun, X. Yu, H. Li and L. Chen, A stabilized PEO-based solid electrolyte via a facile interfacial engineering method for a high voltage solid-state lithium metal battery, *Chem. Commun.*, 2020, **56**(42), 5633–5636.
226 W. Zhou, Z. Wang, Y. Pu, Y. Li, S. Xin, X. Li, J. Chen and J. B. Goodenough, Double-layer polymer electrolyte for high-voltage all-solid-state rechargeable batteries, *Adv. Mater.*, 2019, **31**(4), 1805574.
227 Z. Yao, K. Zhu, X. Li, J. Zhang, J. Li, J. Wang, K. Yan and J. Liu, Double-layered multifunctional composite electrolytes for high-voltage solid-state lithium-metal batteries, *ACS Appl. Mater. Interfaces*, 2021, **13**(10), 11958–11967.

228 X. Yu, J. Li and A. Manthiram, Rational design of a laminated dual-polymer/polymer–ceramic composite electrolyte for high-voltage all-solid-state lithium batteries, *ACS Mater. Lett.*, 2020, **2**(4), 317–324.
229 M. Arrese-Igor, M. Martinez-Ibañez, E. Pavlenko, M. Forsyth, H. Zhu, M. Armand, F. Aguesse and P. López-Aranguren, Toward High-Voltage Solid-State Li-Metal Batteries with Double-Layer Polymer Electrolytes, *ACS Energy Lett.*, 2022, **7**(4), 1473–1480.
230 B. Li, Q. Su, C. Liu, Q. Wang, M. Zhang, S. Ding, G. Du and B. Xu, Stable interface of a high-energy solid-state lithium metal battery via a sandwich composite polymer electrolyte, *J. Power Sources*, 2021, **496**, 229835.
231 S. Mu, W. Huang, W. Sun, N. Zhao, M. Jia, Z. Bi and X. Guo, Heterogeneous electrolyte membranes enabling double-side stable interfaces for solid lithium batteries, *J. Energy Chem.*, 2021, **60**, 162–168.
232 X. Wang, Y. Fang, X. Yan, S. Liu and L. Zhang, Highly conductive polymer electrolytes based on PAN-PEI nanofiber membranes with in situ gelated liquid electrolytes for lithium-ion batteries, *Polymer*, 2021, **3**, 124038.
233 J. Xi and X. Tang, Enhanced lithium ion transference number and ionic conductivity of composite polymer electrolyte doped with organic–inorganic hybrid P123@SBA-15, *Chem. Phys. Lett.*, 2004, **400**(1–3), 68–73.
234 T. Minato, H. Kawaura and M. Hirayama, *et al.*, Dynamic Behavior at the Interface between Lithium Cobalt Oxide and an Organic Electrolyte Monitored by Neutron Reflectivity Measurements, *J. Phys. Chem. C*, 2016, **120**(36), 20082–20088.
235 J. Zheng, C. Sun, Z. Wang, S. Liu, B. An, Z. Sun and F. Li, Double ionic-electronic transfer interface layers for all solid-state lithium batteries, *Angew. Chem., Int. Ed*, 2021, **60**(34), 18448–18453.
236 M. Odziemkowski and D. E. Irish, An Electrochemical Study of the Reactivity at the Lithium Electrolyte/Bare Lithium Metal Interface, *J. Electrochem. Soc.*, 1992, **139**(11), 3063.
237 R. Schmuch, R. Wagner, G. Hrpel, T. Placke and M. Winter, Performance and cost of materials for lithium-based rechargeable automotive batteries, *Nat. Energy*, 2018, **3**(4), 267–278.
238 J. I. Lee, G. Song, S. Cho, D. Y. Han and S. Park, Cover Picture: Lithium Metal Interface Modification for High-Energy Batteries: Approaches and Characterization, *Batteries Supercaps*, 2020, **3**(9), 790.
239 H. Zhou, S. Yu, H. Liu and P. Liu, Protective coatings for lithium metal anodes: recent progress and future perspectives - ScienceDirect, *J. Power Sources*, 2020, **450**, 227632.
240 M. H. Ryou, Y. M. Lee, Y. Lee, M. Winter and P. Bieker, Mechanical Surface Modification of Lithium Metal: Towards Improved Li Metal Anode Performance by Directed Li Plating, *Adv. Funct. Mater.*, 2015, **25**(6), 834–841.
241 T. Wang, J. Duan, B. Zhang, W. Luo, X. Ji, H. Xu, Y. Huang, L. Huang, Z. Song, J. Wen, C. Wang, Y. Huang and J. B. Goodenough, A self-regulated gradient interphase for dendrite-free solid-state Li batteries, *Energy Environ. Sci.*, 2022, **15**(3), 1325–1333.
242 W. Wu, Z. Song, Y. Dai, X. Zheng, G. Chai, J. Yang and W. Luo, Magnetic Actuation Enables Programmable Lithium Metal Engineering, *Adv. Energy Mater.*, 2022, **12**(28), 2200999.
243 J. Becking, A. Grbmeyer, M. Kolek, U. Rodehorst and M. C. Stan, Lithium-Metal Foil Surface Modification: An Effective Method to Improve the Cycling Performance of Lithium-Metal Batteries, *Adv. Mater. Interfaces*, 2017, **4**(16), 1700166.
244 E. P. Kamphaus, S. Angarita-Gomez, X. Qin, M. Shao and P. B. Balbuena, Role of Inorganic Surface Layer on Solid Electrolyte Interphase Evolution at Li-Metal Anodes, *ACS Appl. Mater. Interfaces*, 2019, **11**(34), 31467–31476.
245 J. A. Maslyn, L. Frenck, W. S. Loo, D. Y. Parkinson and N. P. Balsara, Extended Cycling through Rigid Block Copolymer Electrolytes Enabled by Reducing Impurities in Lithium Metal Electrodes, *ACS Appl. Energy Mater.*, 2019, **2**(11), 8197–8206.
246 A. Storelli, S. Rousselot, N. Alzate-Carvajal and V. Pelé, On the Importance of Li Metal Morphology on the Cycling of Lithium Metal Polymer Cells, *J. Electrochem. Soc.*, 2021, **168**(4), 040505.
247 K. J. Harry, D. T. Hallinan, D. Y. Parkinson, A. A. Macdowell and N. P. Balsara, Detection of subsurface structures underneath dendrites formed on cycled lithium metal electrodes, *Nat. Mater.*, 2014, **13**(1), 69–73.
248 A. Etxebarria, S. L. Koch, O. Bondarchuk, S. Passerini, G. Teobaldi and M. Á. Muñoz-Márquez, Work Function Evolution in Li Anode Processing, *Adv. Energy Mater.*, 2020, **10**(24), 2000520.
249 M. M. Markowitz and D. A. Boryta, Lithium Metal-Gas Reactions, *J. Chem. Eng. Data*, 1962, **7**(4), 586–591.
250 W. Irvine and J. Lund, The reaction of lithium with water vapor, *J. Electrochem. Soc.*, 1963, **110**(2), 141.
251 D. Jeppson, J. Ballif, W. Yuan and B. Chou, *Lithium literature review: lithium's properties and interactions*, Hanford Engineering Development Laboratory, 1978.
252 D. David, M. Froning, T. Wittberg and W. Moddeman, Surface reactions of lithium with the environment, *Appl. Surf. Sci.*, 1981, **7**(3), 185–195.
253 J. Hoenigman and R. Keil, An XPS study of the adsorption of oxygen and water vapor on clean lithium films, *Appl. Surf. Sci.*, 1984, **18**(1–2), 207–222.
254 R. A. Rhein, Lithium Combustion: A Review, 1990.
255 K. Zavadil and N. R. Armstrong, Surface chemistries of lithium: detailed characterization of the reactions with O_2 and H_2O using XPS, EELS, and microgravimetry, *Surf. Sci.*, 1990, **230**(1–3), 47–60.
256 K. Wang, P. N. Ross Jr, F. Kong and F. McLarnon, The Reaction of Clean Li Surfaces with Small Molecules in Ultrahigh Vacuum: I. Dioxygen, *J. Electrochem. Soc.*, 1996, **143**(2), 422.
257 C. Skinner, R. Sullenberger, B. E. Koel, M. Jaworski and H. Kugel, Plasma facing surface composition during NSTX Li experiments, *J. Nucl. Mater.*, 2013, **438**, S647–S650.

258 M. Schiemann, J. Bergthorson, P. Fischer, V. Scherer, D. Taroata and G. Schmid, A review on lithium combustion, *Appl. Energy*, 2016, **162**, 948–965.
259 X. He, D. Bresser, S. Passerini, F. Baakes, U. Krewer, J. Lopez, C. T. Mallia, Y. Shao-Horn, I. Cekic-Laskovic and S. Wiemers-Meyer, The passivity of lithium electrodes in liquid electrolytes for secondary batteries, *Nat. Rev. Mater.*, 2021, **6**(11), 1036–1052.
260 S.-K. Otto, T. Fuchs, Y. Moryson, C. Lerch, B. Mogwitz, J. Sann, Jr Janek and A. Henss, Storage of Lithium Metal: The Role of the Native Passivation Layer for the Anode Interface Resistance in Solid State Batteries, *ACS Appl. Energy Mater.*, 2021, **4**(11), 12798–12807.
261 A. Fu, C. Wang, J. Peng, M. Su, F. Pei, J. Cui, X. Fang, J. F. Li and N. Zheng, Lithiophilic and antioxidative copper current collectors for highly stable lithium metal batteries, *Adv. Funct. Mater.*, 2021, **31**(15), 2009805.
262 B. Wen, F. N. Sayed, W. M. Dose, J. K. Morzy, Y. Son, S. Nagendran, C. Ducati, C. P. Grey and M. F. L. De Volder, Surface reduction in lithium- and manganese-rich layered cathodes for lithium ion batteries drives voltage decay, *J. Mater. Chem. A*, 2022, **10**(41), 21941–21954.
263 R. Huang, Y. Ding, F. Zhang, W. Jiang, C. Zhang, P. Yan, M. Ling and H. Pan, The interphasial degradation of 4.2 V-class poly(ethylene oxide)-based solid batteries beyond electrochemical voltage limit, *J. Energy Chem.*, 2022, **75**, 504–511.
264 J. Liu, H. Yuan, H. Liu, C. Z. Zhao, Y. Lu, X. B. Cheng, J. Q. Huang and Q. Zhang, Unlocking the Failure Mechanism of Solid State Lithium Metal Batteries, *Adv. Energy Mater.*, 2021, **12**(4), 2100748.